Lymphatic chain gradients regulate the magnitude and heterogeneity of T cell responses to vaccination

Michael T. Conlon

A dissertation

submitted in partial fulfillment of the

requirements for the degree of

Doctor of Philosophy

University of Washington

2025

Reading Committee:

Michael Y. Gerner, Chair

Jakob Von Moltke

Hao Yuan Kueh

Daniel Campbell

Program Authorized to Offer Degree:

Immunology

University of Washington

Abstract

Lymphatic chain gradients regulate the magnitude and heterogeneity of T cell responses to vaccination

Michael T. Conlon

Chair of the Supervisory Committee:
Michael Y. Gerner
Department of Immunology

Upon activation, T cells proliferate and differentiate into diverse populations, including highly differentiated effector and memory precursor subsets. Initial diversification is influenced by signals sensed during T cell priming within lymphoid tissues. However, the rules governing how cellular heterogeneity is spatially encoded *in vivo* remain unclear. Here, we show that immunization establishes concentration gradients of antigens and inflammation across interconnected chains of draining lymph nodes (IC-LNs). While T cells are activated at all sites, individual IC-LNs elicit divergent responses: proximal IC-LNs favor the generation of effector cells, whereas distal IC-LNs promote formation of central memory precursor cells. Although both proximal and distal sites contribute to anamnestic responses, T cells from proximal IC-LNs preferentially provide early effector responses at inflamed tissues. Conversely, T cells from distal IC-LNs demonstrate an enhanced capacity to generate long-lasting responses to chronic antigens in cancer settings, including after checkpoint blockade therapy. Therefore, formation of spatial gradients across lymphatic chains following vaccination regulates the magnitude, heterogeneity, and longevity of T cell responses.

TABLE OF CONTENTS

LIST OF FIGURES

Non-standard abbreviations: Interconnected Chains of Draining Lymph Nodes (IC-LNs), Vaccine Derived Materials (VDMs), and Non-Draining Lymph Node (ndLN).

ACKNOWLEDGEMENTS

I would first like to thank the mentors who have provided me with the exposure, support, and guidance that allowed me to achieve this milestone. To Dr. Alan Jay Kaufman: thank you for giving me the opportunity to work in your lab as an undergraduate and for introducing me to the world of scientific research. To Dr. Audray Harris: thank you for allowing me to lead my own research project in your lab and for the chance to collaborate with other lab members. The lessons I learned in your lab provided me with a solid foundation that helped me navigate the challenging first years of graduate school. My time in your lab shaped me into a capable researcher, and I will always be grateful for that. To Dr. Michael Gerner: I could not have asked for a better mentor throughout my Ph.D. I am truly thankful for the opportunity to try and fail, as those experiences taught me what it takes to succeed. Even during the times of failure, your passion for science and your commitment to your trainees' success kept the light at the end of the tunnel in sight. I would also like to acknowledge past and present members of the Gerner lab for creating a welcoming and stimulating work environment.

I am deeply grateful to my committee for their unwavering support and guidance throughout the years. It has been an honor to discuss my research with all of you.

To the students, post-docs, and faculty of the UW Immunology program: you have been an integral part of my graduate school experience. I will always appreciate how you have helped me grow not only as a researcher but also as a person. You have shown me that it's okay not to be the smartest person in the room; in fact, it's wise because it means you've surrounded yourself

with the smartest people. Only time will tell, but I truly believe your knowledge and wisdom have rubbed off on me—if only a part of it, it is still more than I ever imagined.

Finally, I would like to thank my family and friends. To my wonderful mom and dad: thank you for always wanting the best for your children, even when it meant making sacrifices on your end. I will never take my upbringing for granted because I know that your unconditional love and support have kept me on the right path. I love you both very much, and I hope to continue making you proud. To my amazing sister Eileen: your dedication to our family's well-being has never wavered, even during difficult times. I will always be in awe of your dedication to pursuing what fulfills you with passion and resilience, and you will forever be an inspiration. To my cousin Steph and her partner Christopher: thank you for being such great friends to me during my time in Seattle. To my aunts and uncles: your unwavering support for your kids, nieces, and nephews has taught me the true meaning of family. My family and upbringing allowed me to make this accomplishment. They are who I am, and I love who they are.

Special thanks to all the mice who make this research possible. Our society is indebted to them.

Chapter 1.

INTRODUCTION

1.1. PROGRESSION OF THE ADAPTIVE IMMUNE RESPONSE

All cellular organisms, whether unicellular or multicellular, are susceptible to a variety of pathogenic threats, including viruses and bacteria. In response, all organisms have developed sophisticated immune systems—a network of molecules, cells, and tissues designed to safeguard against infections. This immune response is generally categorized into two primary systems: the innate immune system and the adaptive immune system, both of which are essential for maintaining health.

The innate immune system represents the more evolutionarily ancient arm of immunity, present in all cellular organisms. It is characterized by its ability to recognize broad patterns shared by many pathogens, known as Pathogen-Associated Molecular Patterns (PAMPs) as well as Damage-Associated Molecular Patterns (DAMPs). For example, in the context of intercellular infections, Toll-like receptor 9 (TLR9), an endosomal protein, can detect methylated DNA (CpG), a feature predominantly associated with bacteria. Upon recognition, TLR9 activation triggers the translocation of transcription factors to the nucleus, leading to the upregulation of pro-inflammatory genes, such as interferons, tumor necrosis factors (TNF) and IL-12. Another example involves the detection of tissue damage by epithelial cells at mucosal surfaces of the gut, which occurs during parasitic worm infections, activating tissue remodeling mechanisms (i.e., the "weep-and-sweep" response) to physically expel the parasite. Although the innate immune system provides rapid and broad-spectrum defense, it traditionally lacks immunological memory, responding similarly to repeated infections. However, emerging evidence suggests a phenomenon

known as “trained immunity,” in which innate immune cells exhibit enhanced responsiveness upon subsequent encounters with pathogens.

The detection of intracellular PAMPs, such as methylated DNA, triggers Type I immunity, in contrast to type II (protection against parasites) or Type III (extracellular and fungal infections) immunity. This study focuses specifically on Type I immunity, which is crucial for defending against intracellular pathogens, such as viruses and bacteria, and forms the basis of immune responses initiated by the majority of commercially available vaccines.

While the innate immune system effectively clears many types of infections, vertebrates have evolved a secondary, more specialized defense: the adaptive immune response. Unlike the innate response, which is triggered by the recognition of PAMPs, adaptive immunity is distinguished by its ability to recognize specific antigens derived from pathogens with high precision. Genetic recombination of the genes encoding T cell and B cell receptors allows for detection of a wide range of pathogen derived antigens. Engagement of these receptors with their cognate antigen results in clonal selection, the rapid proliferation of specific cellular clones able to respond to the same antigen. This allows for a faster and more robust response upon re-exposure to previously encountered pathogens, thus generating immunological memory.

The primary cellular effectors of adaptive immunity are lymphocytes, including both B cells and T cells ($CD4^+$ and $CD8^+$ subsets). Although the antibody-mediated responses of B cells are indispensable for protecting against pathogens, $CD4^+$ and $CD8^+$ T cells play unique and equally critical roles in immune defense and are the main focus of this study. The importance of T cells in

immune protection is starkly illustrated in acquired immunodeficiency syndrome (AIDS), a condition caused by the human immunodeficiency virus (HIV), which selectively targets and depletes $CD4^+$ T cells. As a result, individuals with AIDS become susceptible to a range of otherwise non-lethal, opportunistic infections—underscoring the vital role T cells play in maintaining immune health.

1.2. VACCINES ELICIT LONG LIVED ADAPTIVE IMMUNITY VIA ACTIVATION OF THE INNATE IMMUNE SYSTEM

The generation of long-lived memory lymphocytes underpins the protective effects of vaccines. Although vaccines have revolutionized public health, our understanding of the precise mechanisms by which they elicit adaptive immune memory has largely been based on empirical observations, necessitating further research into the molecular pathways involved in vaccination-induced immune priming. Vaccines encompass a diverse array of platforms, including subunit vaccines (comprising purified proteins or peptides, such as the influenza vaccine), whole organism vaccines (live attenuated or inactivated, e.g., smallpox and poliovirus vaccines), and nucleic acid-based vaccines (e.g., the SARS-CoV-2 vaccines developed in 2020). Despite this heterogeneity, a unifying feature of these formulations is the presence of an antigen, typically delivered in conjunction with an adjuvant to enhance immunogenicity.

Generally, vaccines are administered as either a single or series of intramuscular injections at a peripheral site, such as the upper arm. Following administration, vaccine derived materials (VDMs), including antigens and adjuvants, are captured by local myeloid cells, such as migratory

dendritic cells, which then transport this information to regional lymph nodes via lymphatic vessels. In some cases, vaccine-derived materials may also drain directly into the lymph node, where they are sampled by resident dendritic cells. Dendritic cells are highly effective at responding to adjuvants and processing antigens to display on their surface, thus earning their designation as antigen-presenting cells (APCs). APCs present antigen in the form of peptides in complex with MHC molecules on the cell surface, which activates naïve T cells through their T cell receptor (TCR). Upon activation, naïve T cells undergo clonal proliferation and differentiation into effector T cells, which subsequently migrate to sites of antigen exposure—either the site of immunization or, in the context of infection, the site of pathogen entry. Following the clearance of VDMs or pathogens, the majority of effector T cells undergo apoptosis during the contraction phase of the immune response. However, a subset of these cells persists and differentiates into long-lived memory T cells, which are capable of mounting rapid and robust responses upon re-exposure to the same antigen—whether during reinfection or following vaccination. The generation of durable memory T cell populations is therefore a critical objective of vaccination strategies. Despite their importance, the precise molecular and immunological mechanisms governing the differentiation and maintenance of vaccine-induced memory T cells remain incompletely understood and warrant further investigation.

1.3. T CELL ACTIVATION AND DIFFERENTIATION

Following infection or vaccination, activated antigen-specific T cells undergo clonal expansion and differentiate into diverse subsets, including highly differentiated effector cells and less differentiated cells with enhanced memory potential (Kaech et al., 2003; Krueger et al., 2021; Pais

Ferreira et al., 2020; Soerens et al., 2023; Zhou et al., 2010). This heterogeneity ensures immediate immune defense while enabling rapid recall for effective anamnestic responses. Significant efforts have focused on understanding the factors that guide T cell differentiation. The prevailing model suggests that the cumulative strength of stimulation by antigen, co-stimulatory molecules, and cytokines predominantly shapes T cell outcomes (Chang et al., 2014; Henning et al., 2018; Kaech and Cui, 2012)**.** While increased initial priming signals promote effector differentiation, moderate signal exposure enhances memory response generation (Angelosanto et al., 2012; Baharom et al., 2021; Catron et al., 2006; Joshi et al., 2007; Ozga et al., 2016; Shakiba et al., 2022; Zehn et al., 2009).

Heterogeneity among responding T cells emerges shortly after activation within lymphoid organs, with both effector-like and memory precursor subsets identifiable within several days of priming (Grassmann et al., 2020; Kakaradov et al., 2017; Leal et al., 2021; Pais Ferreira et al., 2020; Utzschneider et al., 2020). Early heterogeneity is accompanied by substantial plasticity, allowing for population convergence upon the cessation of stimulation (Abadie et al., 2024; Badovinac and Harty, 2007; Herndler-Brandstetter et al., 2018; Plumlee et al., 2015; Youngblood et al., 2017). However, early effectors and memory precursor cells exhibit distinct patterns of chemokine receptors and adhesion molecules, fostering divergent trafficking to specific body sites and reinforcing response bifurcation. For example, during type-I inflammation, early effector T cells upregulate T-BET leading to increased expression of CXCR3 (Lord et al., 2005), facilitating rapid repositioning to inflamed sites, where additional exposure to antigens and inflammatory signals further reinforces their effector program (Bangs et al., 2022; Chow et al., 2019; Duckworth et al., 2021; Goldberg et al., 2018; Groom et al., 2012; Hickman et al., 2015; Hu et al., 2011;

Kurachi et al., 2011; Ozga et al., 2022; Prizant et al., 2021). In contrast, central memory precursors express higher levels of CCR7 and CD62L, allowing them to recirculate within secondary lymphoid organs (SLOs) (Graef et al., 2014; Masopust and Schenkel, 2013), thus limiting their exposure to activating stimuli.

Similarly, in chronic infection or cancer settings, large numbers of progenitor exhausted T cells (T_{PEX}), which retain recall capacity, are sequestered within lymphoid organs or dedicated niches inside tumors, while effector T cells migrate to inflamed sites, leading to continued stimulation and eventual differentiation into exhausted T cells (T_{EX}) (Connolly et al., 2021; Dähling et al., 2022; Huang et al., 2022b; Im et al., 2016; Im et al., 2020; Prokhnevska et al., 2023; Schenkel et al., 2021; Utzschneider et al., 2016; Wu et al., 2016). This progressive differentiation model indicates that even the earliest T cell priming events can impact downstream adaptive response outcomes in a determinative fashion.

Single-cell adoptive transfer and cellular barcoding studies have demonstrated substantial heterogeneity in cellular expansion and differentiation among individual T cell clones, even those expressing identical TCRs (Buchholz et al., 2013; Gerlach et al., 2013; Graef et al., 2014). The differentiation patterns of these clones can vary based on specific inflammatory conditions present at the time of activation (Buchholz et al., 2013; Plumlee et al., 2013; Tubo et al., 2013), yet the cumulative sum of these individual clonal responses consistently yield both effector and memory T cells (Mold et al., 2021). *In vivo*, such clonal response heterogeneity likely arises from the stochastic migration of individual antigen-specific naïve T cells across lymphoid organs and activation within distinct tissue microenvironments. However, the stochastic nature of the process

raises the question of whether dedicated mechanisms exist that enable reproducibility in the generation of T cell response outputs during an immune response.

1.4. T CELL PRIMING WITHIN LYMPHATIC CHAINS

Initial T cell priming occurs in lymphatic organs, such as lymph nodes, which are optimized for lymph filtration, antigen capture, and facilitating communication between antigen-presenting dendritic cells (DCs) and recirculating lymphocytes (Cabeza-Cabrerizo et al., 2021; Huang et al., 2022a). LNs are highly organized, featuring distinct microenvironments populated by various innate immune cell subsets (Gerner et al., 2012; Grant et al., 2020; Stoltzfus et al., 2020). Previous studies have shown that subcutaneous immunization with TLR agonists, or infections with lymph-disseminating microbes, elicit robust yet polarized recruitment of IL-12-producing monocytes to areas within the T cell zone that are proximal to the afferent lymphatics (De Koker et al., 2017; Leal et al., 2021; Lian et al., 2020). This creates distinct microenvironments across the draining LN with varying degrees of inflammation, leading to non-equivalent early T cell priming based on the specific sites of activation. Preferential programming of early effector T cells occurs in highly inflamed regions of the tissue, while less differentiated T cells expressing markers of memory precursors are preferentially induced in less inflamed areas within the same organ (Duckworth et al., 2021; Groom et al., 2012; Leal et al., 2021). As a result, T cell heterogeneity can be observed within the proximal draining LN shortly after immunization.

LNs are also arranged into interconnected lymphatic chains that follow the path of interstitial fluid back to the bloodstream (Braun et al., 2011; Oliver et al., 2020). Tracer dye studies

have demonstrated that a single peripheral injection can label multiple interconnected lymph nodes (IC-LNs) (Harrell et al., 2008). While most research has focused on immune responses in LNs nearest the immunization site or in the spleen, several studies have documented vaccine dispersal along lymphatic chains (Irvine et al., 2020; Martin et al., 2021; Yang and Unanue, 2013). This includes evidence from non-human primates receiving lipid nanoparticle RNA vaccines (Hassett et al., 2024; Smedley et al., 2014). The extent of lymphatic dispersal is influenced by vaccine formulation characteristics, such as particle size and surface charge (Irvine et al., 2020). Dispersal of VDMs across IC-LNs likely establishes concentration gradients and distinct inflammatory milieus along the chain. However, whether each LN within a chain generates equivalent immune responses remains an open question.

Chapter 2. INTRODUCTION TO RESULTS

The following is adapted from the following publication:

Conlon, M. T., Huang, J. Y., & Gerner, M. Y. (2025). Lymphatic chain gradients regulate the magnitude and heterogeneity of T cell responses to vaccination. *The Journal of Experimental Medicine*, 222(8), e20241311. https://doi.org/10.1084/jem.20241311. PMID: 40304721 PMCID: PMC12042774

Here, we demonstrate that concentration gradients of VDMs, previously identified in proximal draining LNs (Gerner et al., 2017; Huang et al., 2022a; Leal et al., 2021), extend across interconnected chains of draining LNs, generating additional sites of immune cell activation with varying degrees of local antigen and agonist availability. However, responses within individual IC-

LNs are not equivalent: proximal IC-LNs generate highly differentiated effector T cells, while distal IC-LNs produce less-differentiated T cells expressing markers characteristic of central memory precursor cells. Fate-tracking studies via cellular co-transfers reveal that while cells from both proximal and distal IC-LNs contribute to anamnestic recall responses, they exhibit non-equivalent capacities during chronic antigen exposure in cancer settings. T cells generated in proximal IC-LNs preferentially traffic into tumor tissues and dominate early effector responses, but also display markers of exhaustion and have reduced ability to contribute to long-term response output. Conversely, T cells from distal IC-LNs efficiently populate the tumor-draining LNs, have a preferential ability to generate T_{PEX} cells, and effectively respond to checkpoint blockade therapy.

Chapter 3. INTERCONNECTED LYMPH NODES HAVE DIVERGENT T CELL PRIMING ENVIRONMENTS

Following vaccination, antigens and adjuvants can either drain directly to the nearest lymph node or be transported there by migratory dendritic cells. APCs will then sense adjuvant and process antigen to present to naïve T cells, leading to T cell activation and differentiation. The prevailing theory in the field suggests that the level of stimulation a naïve T cell receives during priming influences its subsequent fate (Kaech and Cui, 2012). Our previous research demonstrated that a single peripheral immunization leads to the polarized recruitment of IL-12 producing inflammatory monocytes within the draining LN (Leal et al., 2021), which is likely due to the increased deposition of VDMs within distinct lobes of the draining LN (Huang et al., 2022a). Indeed, unpublished data from our lab show that the drainage of fluorescently labeled VDMs is polarized, with one lobe of the draining LN being preferentially labeled. Specifically, subcutaneous

immunization on the posterior dorsal side of a mouse with fluorescently labeled OVA results in the labeling of one lobe of the inguinal LN, while ventral immunization labels the adjacent lobe of the same LN (Fig. 3). Importantly, our lab has shown that the spatially heterogeneous recruitment of innate cells directly correlates with the location of distinct effector T cell subsets (T-BET^{HI}) while the areas of lower monocyte recruitment correlates with localized early memory T cell differentiation (TCF-1^{HI}) (Leal et al., 2021). Thus, early T cell activation and differentiation in response to vaccination is, in part, determined by the uneven distribution of VDMs within the lymphatic system.

It is also well-established that LNs are organized into interconnected chains that facilitate the return of interstitial fluid to the circulation (Braun et al., 2011; Oliver et al., 2020). Studies using tracer dyes have shown that a single injection at a peripheral tissue site can robustly label these interconnected LNs (Harrell et al., 2008). Moreover, our unpublished data reveal that a single subcutaneous immunization leads to drainage of fluorescently labeled antigen from the site of immunization to multiple LNs (Fig. 3). It remains to be examined whether this drainage pattern is due to continuous drainage of antigen from one LN to another or simultaneous drainage. Since vaccines are typically administered through a single inoculation at a peripheral site, we hypothesize that, in addition to the nearest draining LN, VDMs may also spread to multiple distal LNs resulting in multiple downstream adaptive T cell responses within these interconnected lymphatic chains.

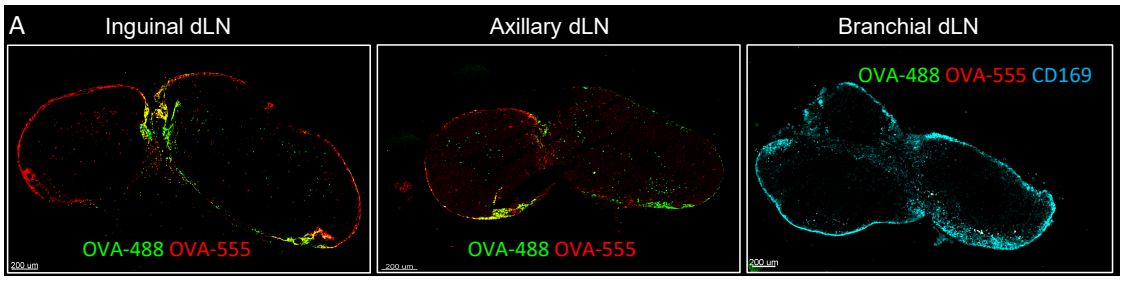

Figure 1. VDMs form gradients across the draining lymph node.

Animals were simultaneously immunized dorsally with 10 μg of OVA-555 and ventrally with 10 μg of OVA-488. 1-day post-immunization, dLNs were isolated, fixed, and sectioned for confocal microscopy. Left: Shows OVA positioning in the inguinal LN after immunization. Middle: Shows positioning of OVA in the distal axillary LN after immunization. Right: Shows OVA positioning in the non-draining branchial LN after immunization, anti-CD169 was used as a surrogate for the morphological outline of the LN (n = 4, 2 experiments).

3.1. VACCINE DERIVED MATERIALS DRAIN ACROSS MULTIPLE IC-LNS POST VACCINATION

We previously demonstrated that VDM dispersal across the draining LN proximal to the site of vaccination can generate spatially localized patterns of innate responses which result in the development of early T cell heterogeneity (Leal et al., 2021). However, VDM dispersal to distal LNs located within the IC-LNs was not examined. To map the path of lymph drainage from the site of vaccination across LNs, we first injected the footpad with a tracer dye, Evans Blue, and examined dye dispersal 30 minutes later (Fig. 2. A). As previously reported (Harrell et al., 2008), we observed robust labeling of the draining popliteal, and to a lesser extent the iliac and inguinal LNs, but not the contralateral LNs, indicating lymphatic connections among these LNs. We next

tested if similar drainage across the chain would occur in vaccination settings. For this, we immunized mice in the footpad with fluorescently conjugated OVA antigen plus CpG (TLR9 agonist) and examined antigen uptake by DCs by flow cytometry 2 hours later (Fig. 2. B-C). We found extensive antigen uptake by both resident and migratory DCs in the proximal popliteal draining LN, as well as throughout the entire LN chain, though the frequency and amount of uptake progressively decreased with increasing distance from the site of immunization. Similar gradient-like pattern of antigen uptake by DCs across both popliteal (proximal) and inguinal (distal) IC-LNs was also evident 24 hours post immunization (Fig. 2. D), indicating that this effect was not transient. Additionally, we found enhanced antigen uptake by DC2s compared to DC1 (Fig. 2.E), consistent with the established role of DC subset positioning within LNs in lymph sampling (Gerner et al., 2017). We did not find differences in the total number of antigen-bearing DCs across the chain (Fig. 2. C), likely reflecting non-equivalent total DC cellularity across organs of varying sizes.

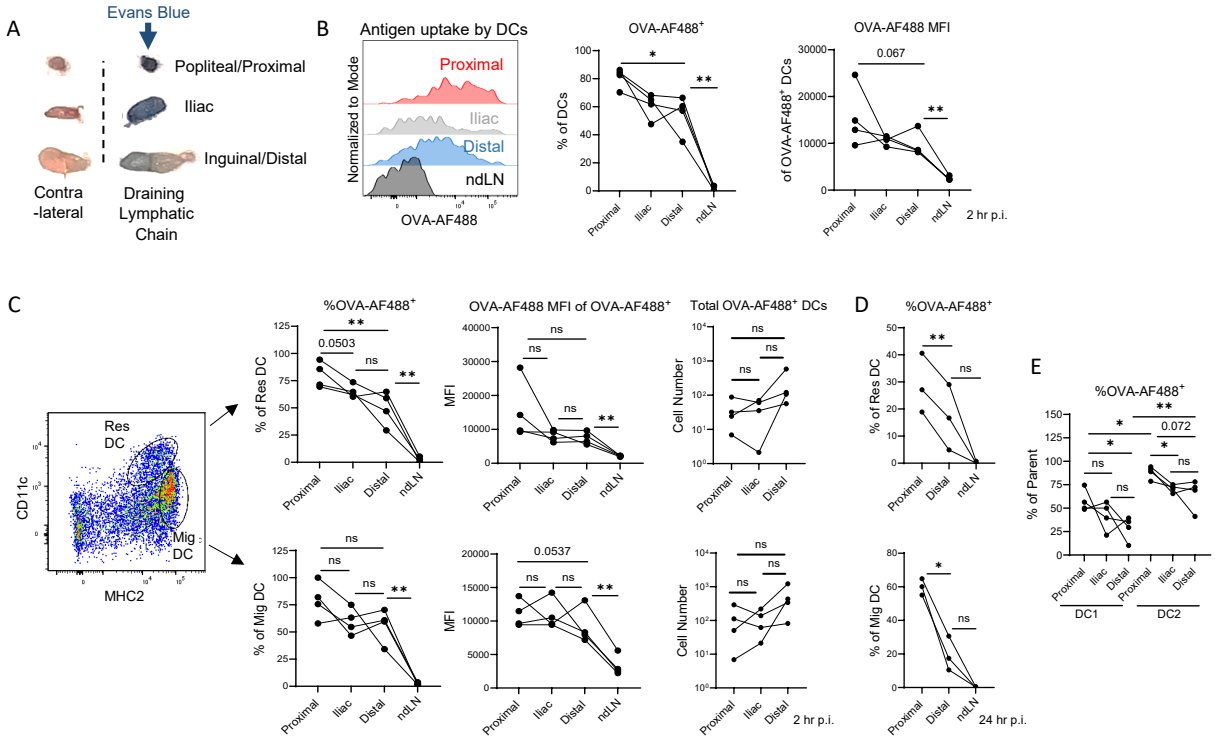

Figure 2. VDMs drain through multiple IC-LNs

(A) B6 mice were injected with Evans Blue in the footpad and 30 minutes later, LNs were harvested to assess drainage (n = 3, 3 experiments). (B) 2 hours post footpad immunization with OVA-AF488 in formulation with CpG, IC-LNs and non-draining contralateral inguinal LNs (ndLN) were harvested to assess antigen uptake by dendritic cells (DCs), defined as $CD11c^{+}MHC2^{+}CD64^{-}B220^{-}Dump^{neg}$ (CD3, NK1.1, Ly6G, Ter119) cells. (C) Representative plot showing gating of migratory (Mig) and resident (Res) DCs, as well as the quantification of OVA-AF488 uptake 2 hours post immunization (n = 4, 2 experiments). (D-E) IC-LNs were harvested 24 hours post immunization (n = 3, 2 experiments). (D) Quantification of OVA-AF488 uptake by migratory and resident DCs 24 hours post immunization. (E) Quantification of antigen uptake by DC1 ($XCR1^{+}CD11b^{-}$ DCs) and DC2 ($CD11b^{+}XCR1^{-}$ DCs) 24 hours post immunization. Interconnected dots represent individual lymphatic chains per mouse. Graphs were analyzed using paired Student's t test. ****$P < 0.0001$; ***$P < 0.001$; **$P < 0.01$; *$P < 0.05$; $P > 0.05$ not significant (ns).

3.2. GENERATION OF INFLAMMATION GRADIENTS ACROSS THE IC-LNS POST VACCINATION

We next examined DC maturation and monocyte recruitment 24 hours post CpG immunization, a timepoint associated with generation of prominent innate responses in LNs following vaccination (Leal et al., 2021; Wu et al., 2024). We found elevated expression levels of costimulatory molecules (CD80, CD86) by migratory DCs and a similar trend for resident DCs across the entire LN chain, but not in contralateral tissues, and the levels of costimulatory molecule expression in distal IC-LNs (iliac, inguinal) was significantly lower as compared to the proximal IC-LN (Fig. 3. A). Enhanced costimulatory molecule expression was particularly evident on DC1s (Fig. 3. B), indicating increased sensitivity to local inflammation. Similarly, we observed enhanced production of IL-12 by DC1s within the popliteal and iliac IC-LNs, but this was markedly abrogated in the distal inguinal IC-LN (Fig. 3. B). Consistent with past findings (De Koker et al., 2017; Leal et al., 2021; Lian et al., 2020; Nakano et al., 2009), we also noted marked recruitment of $Ly6C^{+}CD64^{+}$ inflammatory monocytes to the proximal IC-LN, and a fraction of these cells produced IL-12 (Fig. 3. C-D). While some monocyte recruitment was seen in more distal IC-LNs, this was significantly reduced as compared to proximal sites, and a lower frequency of cells in these distal IC-LNs produced IL-12. Together, these data indicate that footpad immunization leads to marked spread of VDMs across the IC-LNs, although the amount of drainage to different LNs is non-equivalent, leading to the establishment of gradients of antigens and inflammation across the chain.

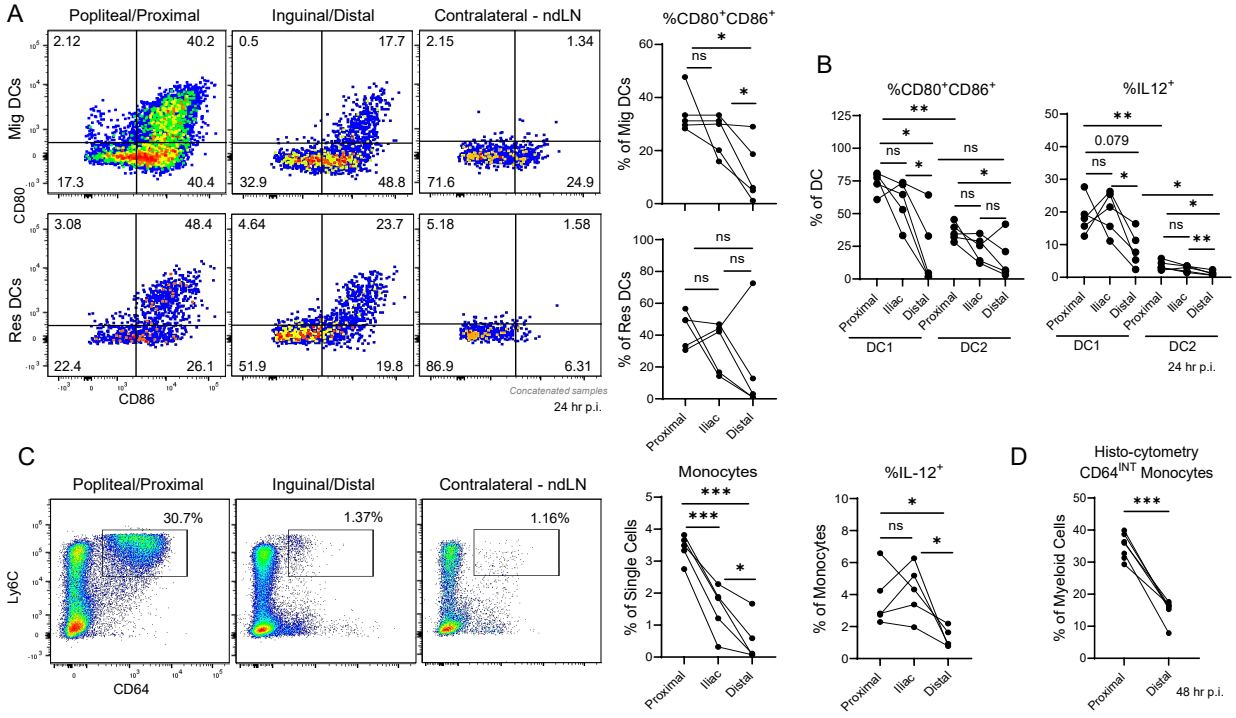

Figure 3. Inflammation gradients across IC-LNs post vaccination.

(A-C) IC-LNs were harvested 24 hours post immunization in the footpad with OVA + CpG. (A) Representative concatenated flow plots and quantifications of CD80 vs. CD86 expression by Migratory (Mig) and Resident (Res) DCs. (B) Quantification of CD80/86 expression and IL-12p40 production by DC1 ($XCR1^{+}CD11b^{-}$ DCs) and DC2 ($CD11b^{+}XCR1^{-}$ DCs) 24 hours post immunization. (C) Representative flow plots and quantification of monocytes across IC-LNs. Monocytes were defined as $Ly6C^{+}CD64^{+}B220^{-}Dump^{neg}$ cells. Quantification of percent monocytes which are $IL12p40^{+}$. (D) Quantification of monocyte representation in the imaged proximal and distal IC-LN tissue sections 48 hours post footpad immunization with OVA + CpG (n = 5, 3 experiments).

3.3. T CELLS ARE ACTIVATED IN DISTINCT PRIMING ENVIRONMENTS ACROSS IC-LNS FOLLOWING VACCINATION

We reasoned that lymphatic gradients across the IC-LNs could impact the local quality of adaptive immune responses to vaccination. To study this, we first visualized early activation of OVA-specific OT-I CD8 transgenic T cells using multiparameter quantitative confocal imaging. Naïve OT-I T cells were adoptively transferred into congenic mice, which were one day later immunized in the footpad with OVA plus CpG, and IC-LNs were harvested 2 days after. Visualization of early T cell activation demonstrated robust induction of Ki67 expression and cellular clustering by OT-I T cells within the T cell zone in both the proximal and distal IC-LNs (Fig. 4. A), indicating rapid activation across the entire chain. However, we also found that T cells activated in proximal IC-LNs had significantly higher IRF4 and pS6 expression (Fig 4. A-B), indicating enhanced TCR signaling (Man et al., 2013; Nayar et al., 2014; Yao et al., 2013), which was consistent with differences in antigen abundance and DC activation across the chain. Furthermore, concurrent visualization of myeloid cell populations demonstrated non-equivalent representation of innate cells within the T cell zones of individual IC-LNs. Consistent with flow cytometry data and past observations (Leal et al., 2021), activated T cells in the proximal IC-LN were embedded within a dense matrix of both CD11c-expressing DCs and CD64-expressing monocytes (Fig. 4. D, Fig 4**.** A, C-D). In contrast, we observed reduced monocyte presence in the T cell zone of distal IC-LNs, and the OT-I T cells in these tissues were primarily associated with DCs. Quantification of these imaging data using CytoMAP cellular spatial correlation analysis (Stoltzfus et al., 2020) indicated a strong positive correlation between activated OT-I T cells and monocytes ($CD64^{INT}$ cells) as well as resident DCs ($CD11c^{+}MHC2^{DIM}CD64^{-}$) in the proximal IC-LNs (Fig. 4. D). In contrast, in distal IC-LNs, there was a marked reduction in the correlation of OT-I T cells with monocytes, and instead there was an increased correlation with $CD11c^{+}MHC2^{HI}CD64^{-}$ DCs. We did not find differences in the spatial correlation between activated OT-I cells and DC1s or DC2s across the

chain (Fig 4. E), indicating equivalent overall positioning of these cell populations in different IC-LNs at 48 hours post immunization. Inflammation can induce the production of inflammatory chemokines, such as CXCL9 and CXCL10, in LNs, which can further modulate cellular responses (Duckworth et al., 2021; Groom et al., 2012). Consistent with this, we observed increased CXCL9 expression in proximal IC-LNs, both across entire tissue sections and specifically within the T cell zone (Fig. 4. F). Together, these findings indicate the presence of non-equivalent priming environments for T cells across the lymphatic chain.

Importantly, quantitative imaging of transcription factors associated with T cell differentiation in CD8 T cells at early stages of activation (48 hours post immunization) demonstrated marked up-regulation of the transcription factor T-BET in many cells within proximal IC-LNs (Fig. 4. G), indicating efficient effector differentiation (Joshi et al., 2007). In contrast, most T cells in distal IC-LNs had reduced T-BET expression, and instead expressed higher levels of TCF1, a transcription factor associated with T cell memory (Zhou et al., 2010).

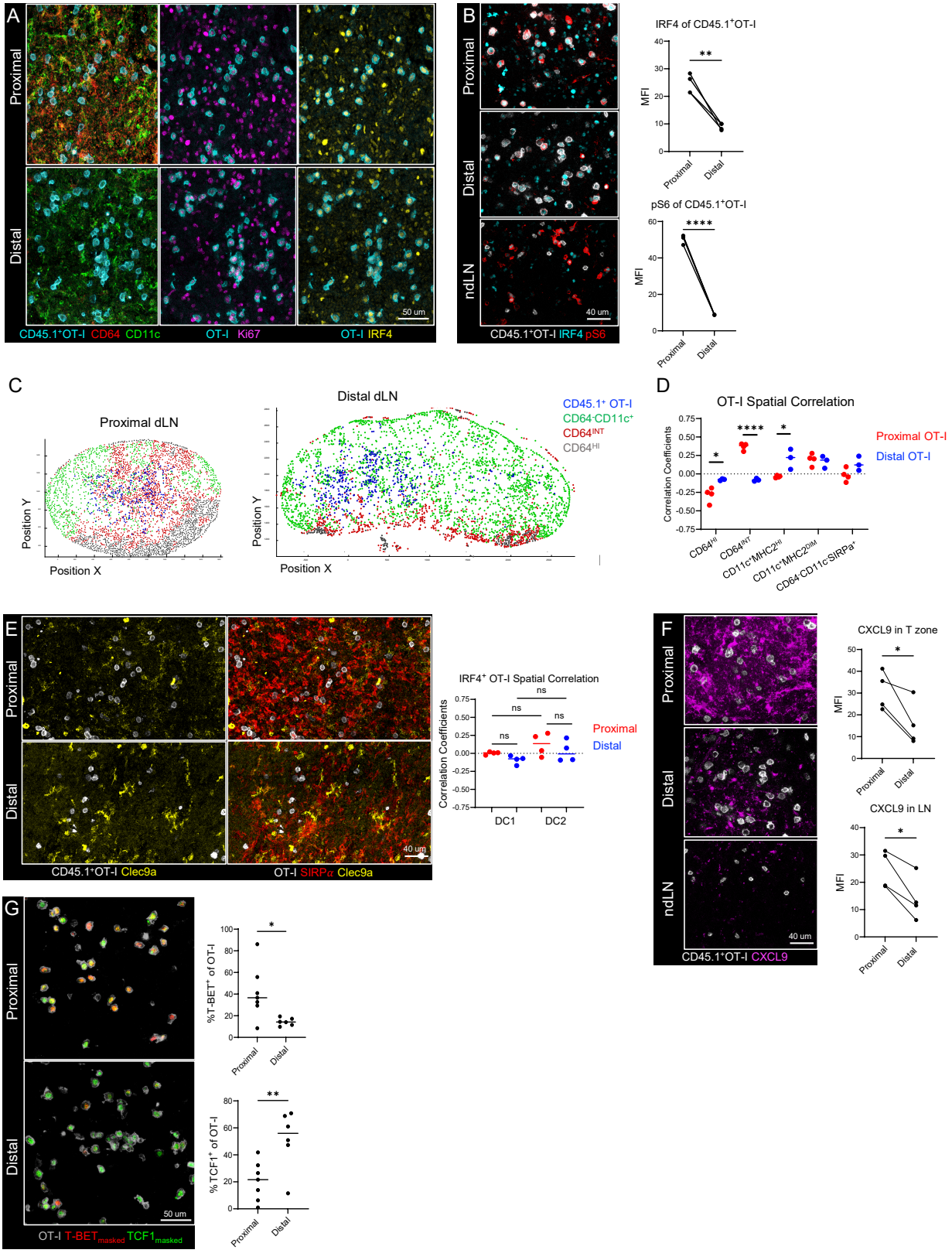

Figure 4. T cells are primed in distinct IC-LN environments.

Naïve CD45.1^{+} OT-I were transferred into naïve CD45.2^{+} mice, which were one day later immunized in the footpad with OVA + CpG. 2 days post immunization, proximal and distal IC-LNs were harvested for analysis by confocal microscopy (n = 5, 3 experiments). (A) Representative images of the indicated markers across the IC-LNs. (B) Representative images of indicated markers across the IC-LNs. Quantification of pS6 and IRF4 expression by the activated (IRF4^{+}) OT-I T cells (C) Spatial distribution maps demonstrating the positioning of indicated myeloid cells and activated (IRF4^{+}) CD45.1^{+} OT-I T cells. (D) Quantification of cell-cell spatial correlations of activated OT-I CD8 T cells with the indicated myeloid cell populations across different IC-LNs. (E) Representative images of indicated markers across the IC-LNs and quantification of cell–cell spatial correlation analysis of activated (IRF4^{+}) CD45.1^{+} OT-I T cells in relation to DC1 (Clec9a^{+}SIRPα^{-}CD11c^{+}CD64^{-} cell objects) and DC2 (SIRPα^{+}Clec9a^{-} CD11c^{+}CD64^{-} cell objects). (F) Representative images and quantification of CXCL9 production within the LN and T cell zone. (G) Representative image and quantification of T-BET and TCF1 expression by the activated OT-I CD8 T cells. T-BET and TCF1 signal was first masked within activated (IRF4^{+}CD45.1^{+}) OT-I T cells for visual clarity.

3.4. PROXIMAL AND DISTAL T CELLS HAVE DIFFERENTIAL RATES OF PROLIFERATION FOLLOWING ACTIVATION

To further examine how these early priming differences impact downstream T cell responses, we transferred carboxyfluorescein succinimidyl ester (CSFE)-labeled OVA-specific naïve OT-I CD8 and OT-II CD4 T cells into recipient mice and immunized these mice one day later. 2 days post immunization, we also treated animals with FTY720 to block T cell egress from the draining LNs in which they were primed in (Mandala et al., 2002). Draining IC-LNs and non-draining LNs were harvested 4 days post immunization and analyzed by flow cytometry. We observed that across all IC-LNs, both CD8 OT-I and CD4 OT-II T cells underwent extensive activation and clonal expansion, as indicated by increased cellularity, CFSE dilution, and expression of CD44 and Ki67

(Fig. 5. A-C). Notably, T cells in the distal (inguinal) IC-LNs underwent fewer cell divisions (as measured by CFSE dilution), demonstrated reduced Ki67 expression in the proliferating cells, and had moderately reduced total cell counts, together being consistent with the overall reduced antigen abundance and DC maturation in these distal sites.

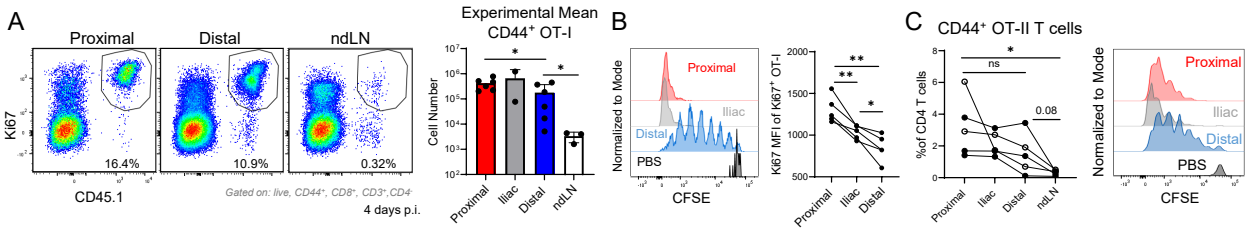

Figure 5. Proximal and distal T cells proliferate at different rates.

CFSE-labeled naïve CD45.1$^+$ OT-I CD8 and OT-II CD4 T cells were transferred into CD45.2$^+$ B6 mice and 1 day later, the mice were immunized with OVA + CpG. Starting 2 days post immunization, mice were treated daily with FTY720. IC-LNs were harvested 3-4 days post immunization for analysis by flow cytometry (n = 4 – 5, 4 experiments). (A) Representative flow plots and quantification of mean cellularity of activated (Ki67$^+$CD44$^+$) OT-I T cells across multiple experiments are shown. Dots represent individual experimental means. (B) Representative CFSE dilution plot for activated OT-I T cells across IC-LNs. OT-I T cells from PBS immunized mice were used as a negative control. Summary graphs show quantification of Ki67 gMFI within Ki67$^+$ OT-I T cells. (C) Cellular frequencies and representative CFSE dilution plots for CD44$^+$ OT-II CD4 T cells. Interconnected dots represent individual lymphatic chains per mouse. Data from multiple pooled experiments are denoted by different symbols within the same group. Graphs show mean ± SD and were analyzed using paired Student's t test. ****P < 0.0001; ***P < 0.001; **P < 0.01; *P < 0.05; P > 0.05 not significant (ns).

3.5. HETEROGENEITY IN EARLY CD4 AND CD8 T CELL RESPONSES ACROSS THE LYMPHATIC CHAIN.

We next examined the differentiation properties of T cells activated in different LNs. As seen in past studies (Leal et al., 2021) and consistent with the imaging data (Fig. 4. G), both CD8 and CD4 T cells in proximal (popliteal) IC-LNs underwent robust early differentiation into two main populations: highly differentiated (T-BET^{+}TCF1^{-}) effector cells and less differentiated (T-BET^{INT}TCF1^{+}) subsets (Fig. 6. A-B). In contrast, T cells isolated from distal inguinal IC-LNs exhibited increased TCF1 and reduced T-BET expression. Consistent with increased T-BET expression, we observed non-equivalent cytokine production after *ex vivo* re-stimulation, with OT-I T cells generated in proximal IC-LNs producing significantly greater amounts of IFNγ and Granzyme B as compared to their counterparts in distal IC-LNs (Fig. 6. A). Large frequencies of activated OT-I and OT-II T cells in proximal but not distal IC-LNs also had elevated expression of the IL-2 receptor alpha chain, CD25, and some OT-I T cells expressed KLRG1 (Fig. 6. C-D), together suggesting divergent effector differentiation across the chain (Sarkar et al., 2008; Kalia et al., 2010; Ruterbusch et al., 2020). Notably, we also observed enhanced expression of immune-regulatory molecules, PD1 and TIM3, in proximal IC-LNs, and these were not elevated in the distal tissues (Fig. 6. E-F). These data indicate that enhanced activation and effector differentiation of T cells in proximal IC-LNs is also accompanied with expression of inhibitory factors, which could in turn counterbalance downstream responses (Avery et al., 2018; Johnnidis et al., 2021; Wei et al., 2013; Wherry and Kurachi, 2015). In addition, we found that responding T cells across the LN chains exhibited divergent patterns of trafficking molecule expression. Most OT-I and OT-II T cells in proximal IC-LNs lacked CD62L expression while displaying increased levels of CXCR3, and CX3CR1 for OT-I T cells (Fig. 6. G-H), altogether indicating induction of effector or effector memory precursor cells with enhanced ability to traffic to sites of inflammation (Duckworth et al., 2021; Zwijnenburg et al., 2023). In contrast, a larger frequency of T cells in distal inguinal IC-LNs

expressed CD62L and exhibited modestly, but significantly, reduced levels of CXCR3 (as measured by geometric mean fluorescence intensity; gMFI), suggesting enhanced lymphoid organ trafficking potential. Of note, we also observed increased expression of $\beta 7$ integrin and CCR9 on OT-I T cells generated in iliac LNs (Fig. 6. I), indicating additional differences in T cell programming based on LN subtype (Iwata et al., 2004). Notably, differences in effector differentiation persisted even without FTY720 treatment, strongly indicating that early phenotypic outcomes were not merely artifacts of artificially retaining T cells in the lymph node during priming (Fig. 6. J).

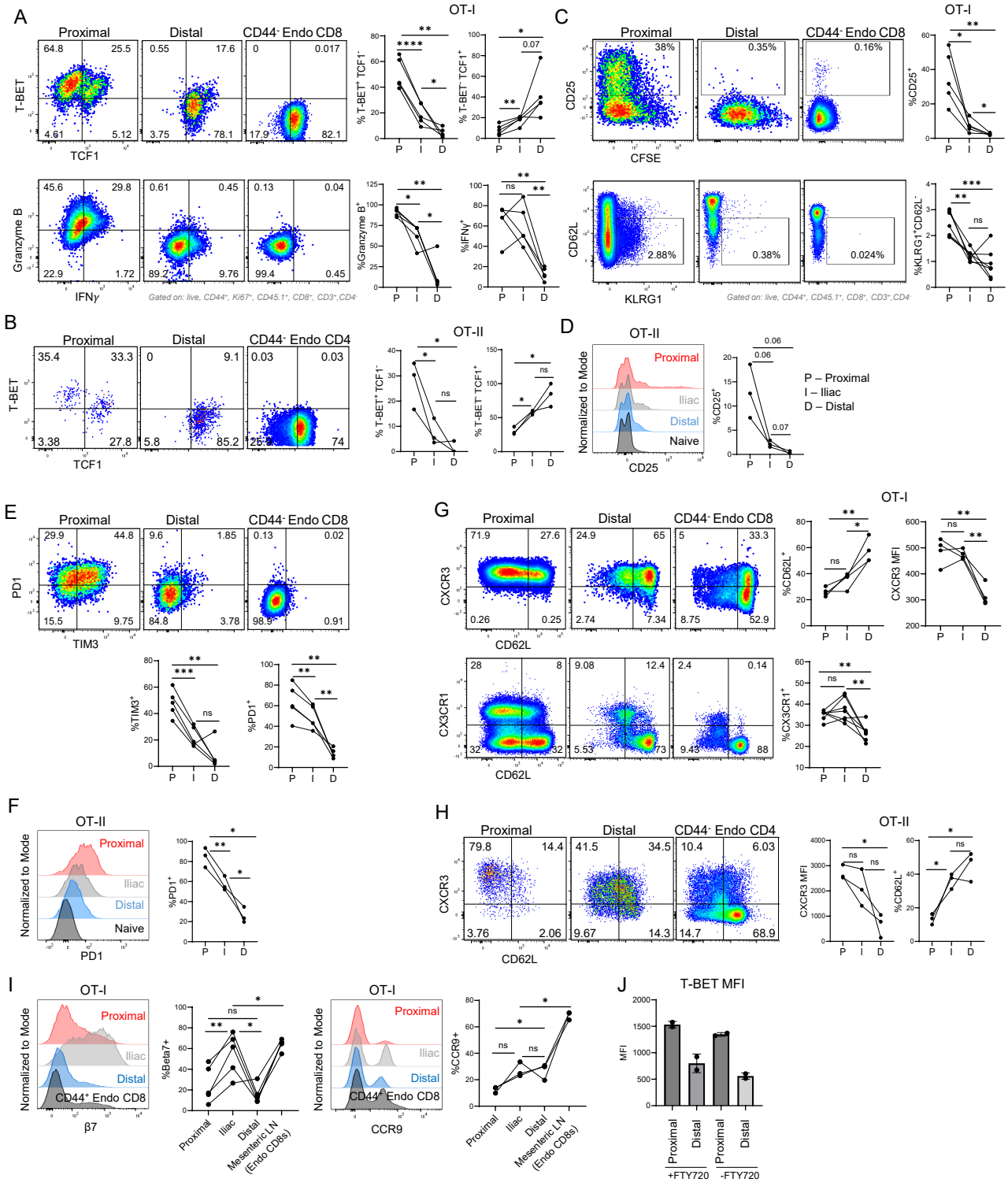

Figure 6. Early heterogeneity in CD4 and CD8 T cells responses across the lymphatic chain.

CFSE-labeled naïve CD45.1^{+} OT-I CD8 and OT-II CD4 T cells were transferred into CD45.2^{+} B6 mice and 1 day later, the mice were immunized with OVA + CpG. Starting 2 days post immunization, mice were treated daily with FTY720. IC-LNs were harvested 3-4 days post immunization for analysis by flow cytometry (n = 4 – 5, 4 experiments). (A-I) Representative flow plots and quantification showing the indicated surface marker or transcription factor staining and cytokine production post ex vivo re-stimulation by the activated OT-I and OT-II T cells, or naïve (CD44^{-}) endogenous CD8 or CD4 T cells. (J) Quantification of T-BET MFI by activated OT-I T cells 4 days post immunization with or without FTY720 treatment (n = 2/group, 1 experiment). Interconnected dots represent individual lymphatic chains per mouse. Graphs were analyzed using paired Student's t test. ****P < 0.0001; ***P < 0.001; **P < 0.01; *P < 0.05; P > 0.05 not significant (ns).

3.6. HETEROGENEITY IN EARLY T CELL RESPONSES ACROSS THE LYMPHATIC CHAIN OCCURS POST INTRAMUSCULAR IMMUNIZATION AND IS DOSE INDEPENDENT.

To examine T cells responses across IC-LNs following additional vaccination routes, we performed intramuscular (i.m.) immunizations in the hind leg of OT-I recipient mice. This again resulted in marked T cell activation in popliteal (proximal), iliac, and inguinal (distal) IC-LNs, as compared with non-draining contralateral LNs and PBS injected controls (Fig. 7. A). Similar to footpad immunizations, we observed increased Ki67 expression in CD8 T cells activated in proximal IC-LNs, albeit this did not result in numerical differences in OT-I T cells across the tissues. Importantly, T cells activated in proximal IC-LNs again demonstrated markedly elevated levels of T-BET, IFNγ, and CD25 expression (Fig. 7. B), suggesting enhanced effector differentiation in proximal as compared to distal IC-LNs, and indicating that divergent patterns of activation were not unique to cutaneous immunization. Additionally, we tested whether antigen

dosing could influence T cell responses across the lymphatic chain using low (1ug) and ultra-low (0.1ug) doses of OVA. As expected, immunizations with lower antigen doses resulted in reduced overall T cell activation and proliferation (Fig. 7. C). Importantly, for all antigen doses, we again observed increased expression of T-BET and IFNγ in OT-I CD8 T cells in proximal popliteal as compared to distal IC-LNs (Fig. 7. D), indicating divergent T cell effector differentiation across the lymphatic chain.

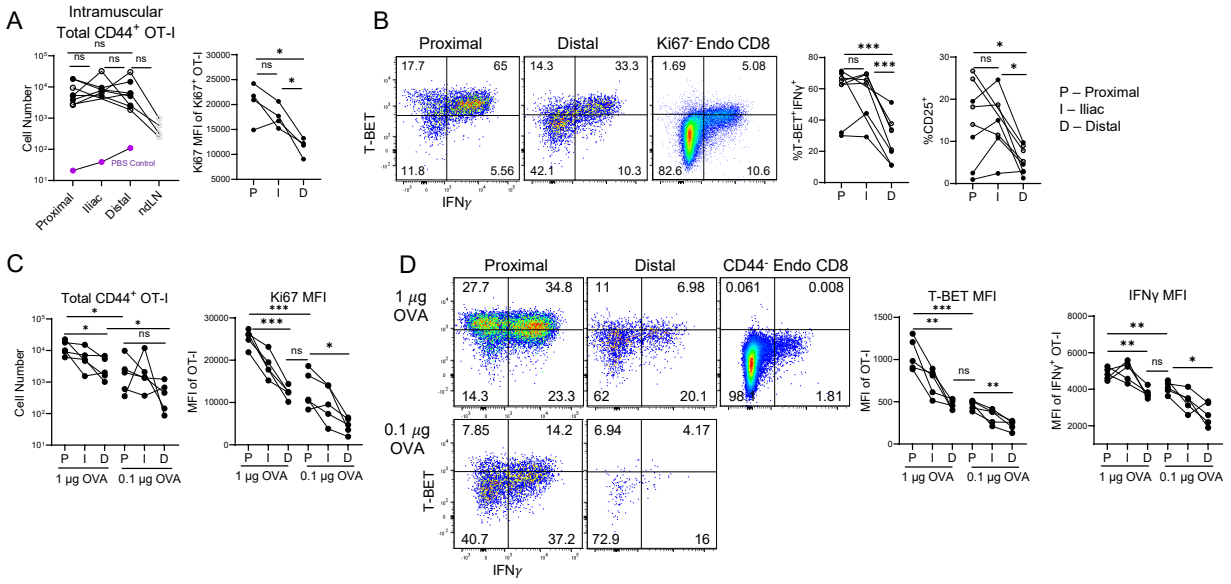

Figure 7. Early heterogeneity post intramuscular immunization and is dose independent.

(A-B) Mice were adoptively transferred with CD45.1$^+$ OT-I CD8 T cells and one day later, intramuscularly immunized with OVA plus CpG. Starting 2 days post immunization, mice were treated with FTY720. IC-LNs were harvested 4 days post immunization for analysis by flow cytometry (n = 4 mice, 2 experiments). (A) Quantification of cellularity of activated OT-I T cells and quantification of Ki67 gMFI within Ki67$^+$ OT-I T cells. (B) Representative flow plots and quantification of indicated marker expression and IFNγ production following re-stimulation by activated OT-I T cells or Ki67$^-$ endogenous CD8 T cells. (C-D) Analysis of cellularity and Ki67 for CD44$^+$ OT-I T cells 4 days after footpad immunization with either 1 µg or 0.1 µg OVA in

formulation with 20 µg CpG (n = 5, 2 experiments). (D) Representative flow plots and quantification of T-BET expression and IFNγ production following ex vivo re-stimulation.

3.7. INNATE STIMULATING ADJUVANTS ARE REQUIRED FOR PROPER EFFECTOR DIFFERENTIATION

Increased generation of effector responses in proximal IC-LNs was consistent with presence of elevated inflammatory microenvironments due to gradient-like dispersal patterns of adjuvant across the lymphatic chain. Indeed, exclusion of the adjuvant, CpG, from the formulation resulted in reduced overall T cell expansion, as well as abrogated expression of CD25 and CXCR3, and elevated CD62L expression in responding T cells in the proximal IC-LNs (Fig. 8. A). This demonstrated that, as expected (Pulendran et al., 2021), presence of adjuvant was critical for induction of T cell effector differentiation in draining LNs.

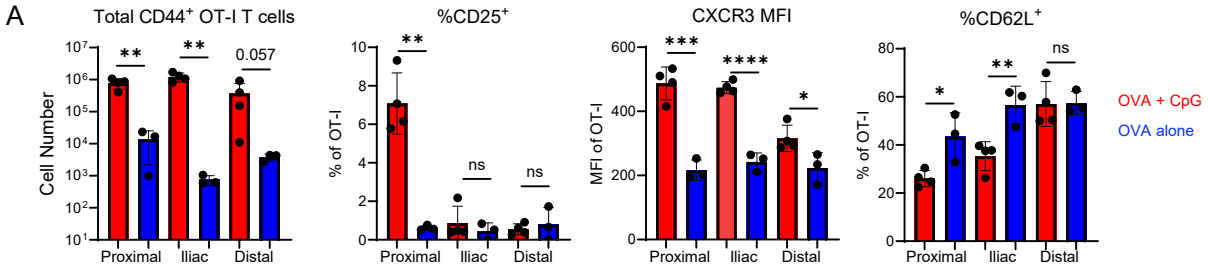

Figure 8. Innate stimulating adjuvants drive proper effector differentiation across IC-LNs.

(A) As described in Fig. 2.4. Quantification of the total cell number of and expression of the indicated markers by the activated OT-I T cells across IC-LNs following immunization with OVA, with or without inclusion of CpG adjuvant (n = 3 – 4, 2 experiments).

3.8. LYMPHATIC CHAIN-BASED PROGRAMMING OF T CELL RESPONSES WITH DISTINCT VACCINE FORMULATIONS.

Given that OVA and CpG are both soluble molecules, we next tested whether other commonly used vaccine adjuvants, including particulate (Alum plus LPS; AS04 analogue) and oil-in-water nano-emulsion (AddaVax; MF59 analogue) formulations (Zhao et al., 2023), also elicit heterogeneous responses across the lymphatic chain (Fig. 9. A-D). For both adjuvants, we observed robust OT-I CD8 T cell clonal expansion across the chain, and in contrast to the soluble formulation, the total numbers of OT-I CD8 T cells within the individual IC-LNs were largely equivalent (Fig. 9. A, C). Importantly, similar to CpG studies, both Alum plus LPS and AddaVax adjuvants elicited non-equivalent effector differentiation in distinct LNs. In proximal IC-LNs, we observed enhanced generation of highly differentiated T-BET^{+}TCF1^{-} effector or effector memory precursor T cells, while a higher frequency of T-BET^{-}TCF1^{+} cells was found in distal IC-LNs (Fig. 9. B, D). Similarly, there was preferential generation of CD25-expressing T cells in proximal IC-LNs, and conversely an increase in CD62L-expressing cells in distal tissues. Differences in CXCR3 expression across sites were less clear with these formulations.

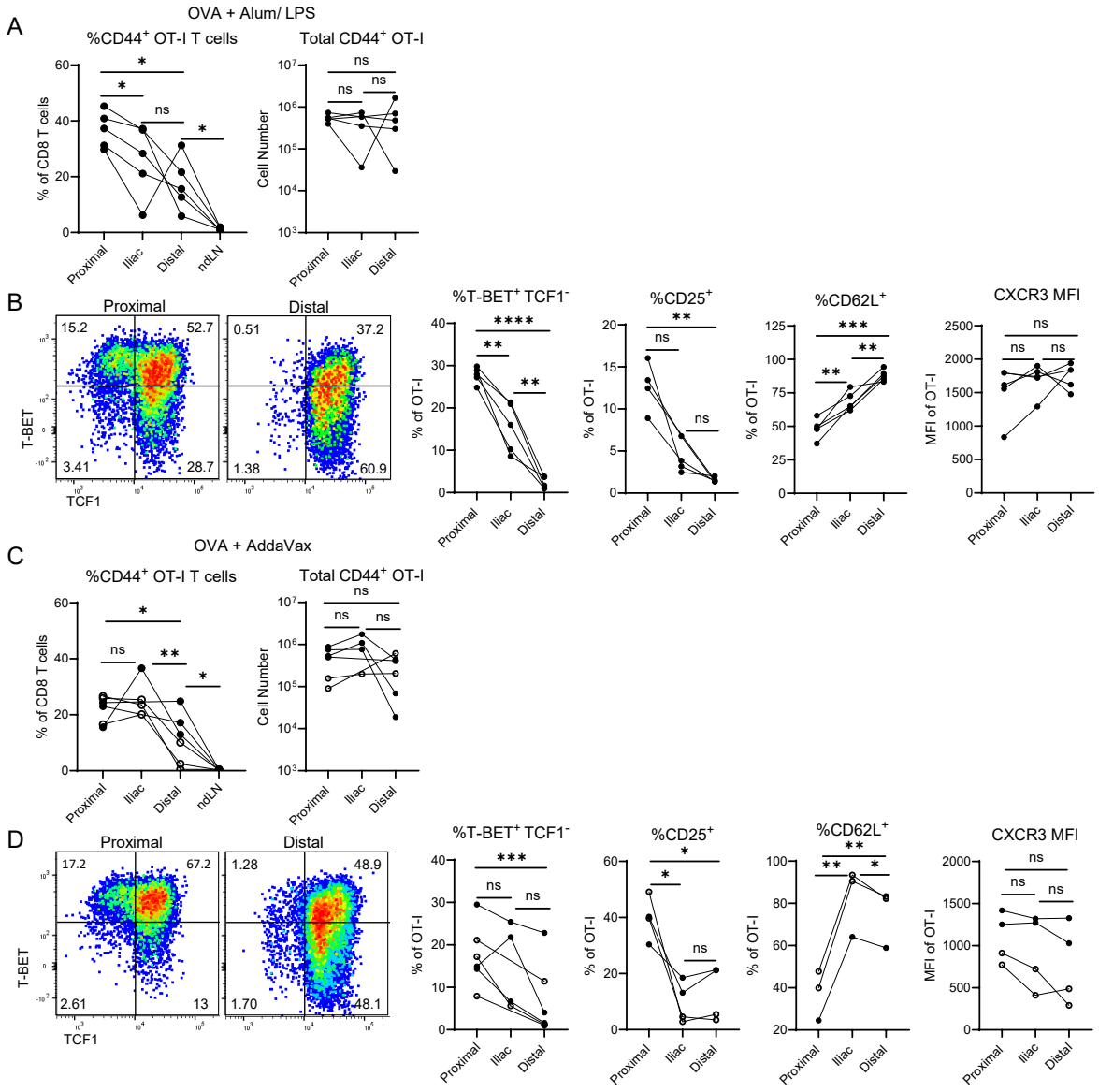

Figure 9. Various vaccine formulations result in lymphatic chain-based priming of T cells.

(A-D) Cellularity and phenotypic analysis of CD44^{+} OT-I T cell responses 4 days after immunization with OVA formulated with A, B) Alhydrogel + LPS (Alum/LPS) or C, D) AddaVax (n = 3 – 4, 2 experiments). Data from multiple pooled experiments are denoted by different symbols within the same group. Interconnected dots represent individual lymphatic chains per mouse. Graphs were analyzed using paired Student's t test for comparison within the same mouse or un-paired between separate mice. ****P < 0.0001; ***P < 0.001; **P < 0.01; *P < 0.05; P > 0.05 not significant (ns).

3.9. POLYCLONAL CD8 ARE ACTIVATED ACROSS IC-LNS YET ALSO DISPLAY DIVERGENT EFFECTOR DIFFERENTIATION

We next evaluated whether these findings extend to endogenous CD8 T cell responses. For this, mice were immunized in the footpad with OVA plus CpG, treated with FTY720, and the IC-LNs were harvested 4 days later and analyzed for OVA-specific CD8 T cell responses using Kb-OVA (SIINFEKL) tetramers. We observed marked and equivalent numerical expansion of OVA-specific CD8 T cells across all IC-LNs downstream of the immunization site (Fig. 10. A-B), suggesting potent cellular activation. Notably, activated CD8 T cells across the chain again displayed non-equivalent effector differentiation patterns, with preferential expression of T-BET and CD25 by activated cells in proximal IC-LNs, and with a higher frequency of cells being T-BET^{-}TCF1^{+} in distal sites (Fig. 10. C-D). In addition, T cells from proximal IC-LNs had increased expression of IRF4 (Fig. 10. D), consistent with increased antigen sensing and effector differentiation (Yao et al., 2013). We also found differences in homing molecule expression by Kb-OVA binding CD8 T cells, with significantly increased representation of CD62L-positive cells in distal IC-LNs, and with a converse non-significant trend in increased CXCR3 expression for T cells activated in proximal tissues (Fig. 10. E). Altogether, these data indicate that vaccination via diverse routes induces potent but non-equivalent responses of both CD4 and CD8 T cells across the lymphatic chain, with enhanced generation of effector and effector memory precursor cells in proximal IC-LNs and predominant induction of central memory precursor responses in distal IC-LNs.

We also examined polyclonal OVA-specific CD8 T cell responses using the Alum plus LPS particulate formulation. We observed robust induction of T cell responses across the chain and equivalent numerical expansion within individual IC-LNs (Fig. 10. F). Importantly, cells in different sites again had non-equivalent differentiation properties. Higher frequencies of T cells generated in proximal IC-LNs expressed T-BET^{+}TCF1^{-} and were CD25^{+}, while more T cells in distal IC-LNs expressed TCF1 (Fig. 10. G), and we also observed non-significant trends in CD62L expression (Fig. 10. H). Altogether, these data show that diverse subunit vaccine formulations elicit potent yet highly heterogeneous patterns of early T cell responses across the lymphatic chains.

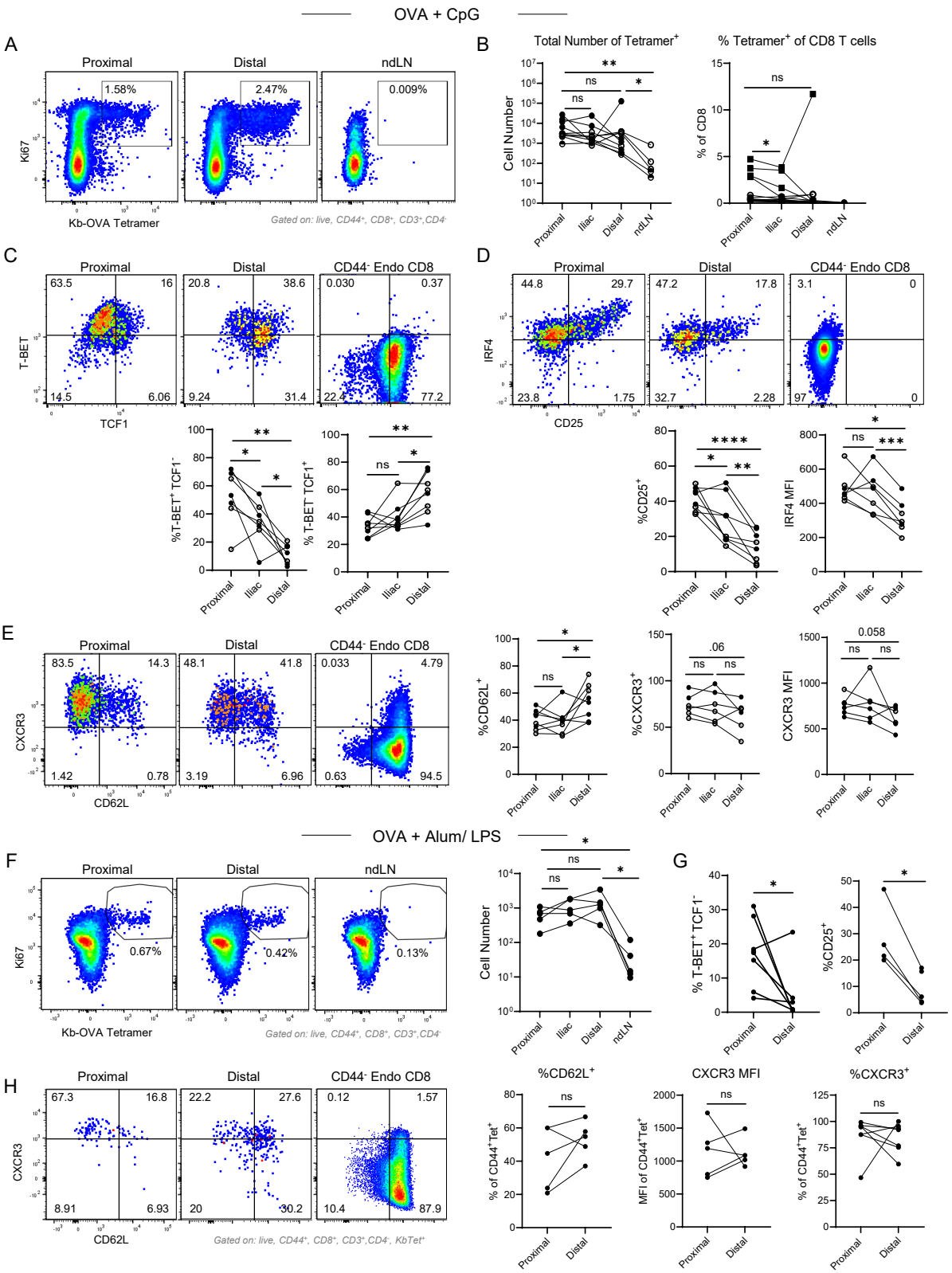

Figure 10. Early heterogeneity in polyclonal CD8 T cell responses.

(A-E) B6 mice were immunized in the footpad with OVA + CpG, FTY720 treated on days 2 and 3, and the IC-LNs were analyzed for endogenous CD8 T cell responses using Kb-OVA tetramers (Kb-SIINFEKL) 4 days post immunization (n = 4 – 5, 4 experiments). (A) Representative plots demonstrating detection of OVA-tetramer$^+$ CD8 T cells across IC-LNs and non-draining LN (ndLN). Cells were first gated on CD3$^+$CD8$^+$CD4$^-$CD44$^+$Ki67$^+$ live singlets. (B) Quantification of percent and total cell number of activated OVA-tetramer$^+$ CD8 T cells across LNs. (C-E) Representative flow plots and quantification of the indicated transcription factor or surface marker expressed by the activated OVA-tetramer$^+$ CD8 T cells. (F-H) Mice were immunized with OVA in formulation with Alum/LPS, as well as treated with FTY720 starting day 2. 4 days post immunization, the F) total number of activated OVA-tetramer$^+$ CD8 T cells and G-H) expression of the indicated markers by OVA-tetramer$^+$ cells was quantified (n = 5, 2 experiments). Interconnected dots represent individual lymphatic chains per mouse. Data from multiple pooled experiments are denoted by different symbols within the same group. Graphs were analyzed using paired Student's t test. ****P < 0.0001; ***P < 0.001; **P < 0.01; *P < 0.05; P > 0.05 not significant (ns).

Chapter 4. EARLY DIFFERENCES IN T CELL DIFFERENTIATION TRANSLATE TO DOWNSTREAM FUNCTIONAL DIFFERENCES BETWEEN PROXIMAL AND DISTAL IC-LN DERIVED T CELLS

During infections, T cells would normally exit the LN of priming in a S1PR-dependent manner (Mandala et al., 2002). From there, they eventually enter the bloodstream and traffic to the site of infection. Once at the infection site, continuous sensing of antigen and inflammation promotes further terminal effector differentiation of T cells (Bangs et al., 2022; Chow et al., 2019; Duckworth et al., 2021; Goldberg et al., 2018; Groom et al., 2012; Hickman et al., 2015; Hu et al., 2011; Kurachi et al., 2011; Ozga et al., 2022; Prizant et al., 2021). After clearance of infection or VDMs, a contraction phase follows, during which most effector T cells undergo apoptosis. This

leaves behind a small population of long-lived memory T cells that can respond to secondary infection or, in the case of vaccination, primary infection (Kaech and Cui, 2012). While some studies have observed plasticity in the ability of terminally differentiated T cells to contribute to the long-lived memory pool (Abadie et al., 2024; Badovinac and Harty, 2007; Herndler-Brandstetter et al., 2018; Plumlee et al., 2015; Youngblood et al., 2017), it is generally believed that further-differentiated effector T cells – especially terminally differentiated one – are more likely to undergo apoptosis during the contraction phase. In contrast, less differentiated memory precursor T cells form the majority of the long-lived memory T cell pool (Grassmann et al., 2020; Kakaradov et al., 2017; Leal et al., 2021; Pais Ferreira et al., 2020; Utzschneider et al., 2020). Additionally, previous studies have demonstrated that T cells that undergo terminal effector differentiation during the acute phase of infection have poor ability to persist when transferred into chronically infected mice (Angelosanto et al., 2012). Building on this, more recent studies have detected the presence of long-lived T_{PEX} cells that effectively respond to PD-1 therapy during the earliest stages of chronic antigen (McManus et al., 2025). Together, these studies suggest that the pathways that dictate effector differentiation during acute infection are similar to those that dictate exhaustion in response to chronic antigen sensing. Based on the early phenotypic divergence of T cells generated across the IC-LN, we hypothesized that T cells derived from either proximal or distal IC-LNs would have distinct downstream fates dependent on the LN of origin.

4.1. DISTAL IC-LN DERIVED T CELLS HAVE REDUCED IMMEDIATE PROLIFERATION RATE

Recent evidence indicates that central memory precursor cells have reduced cycling rates as compared to effector and effector memory populations (Kretschmer et al., 2020). Therefore, we assessed the immediate proliferative properties of OT-I cells derived from proximal versus distal IC-LNs after isolation from their initial priming environments. To do this, naïve OT-I CD8 T cells were transferred into mice, which were then immunized with OVA plus CpG together with FTY720 treatment (as above). Four days post immunization, OT-I CD8 T cells from proximal (popliteal) or distal (inguinal) IC-LNs were isolated, labeled with CFSE, and re-transferred in equal numbers into separate cohorts of secondary naïve recipient mice. One day later, LNs (pooled) and spleens from these recipients were harvested for flow cytometry analysis (Fig. 11. A). Quantification of cellular recovery revealed a numerical advantage for proximal IC-LN derived T cells over those derived from distal IC-LNs, although notably, this difference was most prominent in the spleen and was not significant in LNs (Fig. 11. B). We also observed a significant decrease in CFSE gMFI (enhanced proliferation) and increased Ki67 expression for proximal IC-LN derived OT-I T cells in the spleen, and a similar but non-significant trend in LNs (Fig. 11. C-D). In addition, we noted an increased frequency of proximal IC-LN derived T cells being positive for active caspase 3 staining (Fig. 11. E), suggesting increased cell death. No difference in the expression of anti-apoptotic molecule, BCL2, was observed between proximal and distal IC-LN-derived cells (Fig. 11. F). Together, these findings demonstrate that after immediate re-transfer into naïve recipients and in the absence of additional antigen and inflammation, proximal IC-LN derived T cells continue to undergo enhanced proliferation as compared to their distal IC-LN-derived counterparts, albeit this is also associated with increased rates of cell death.

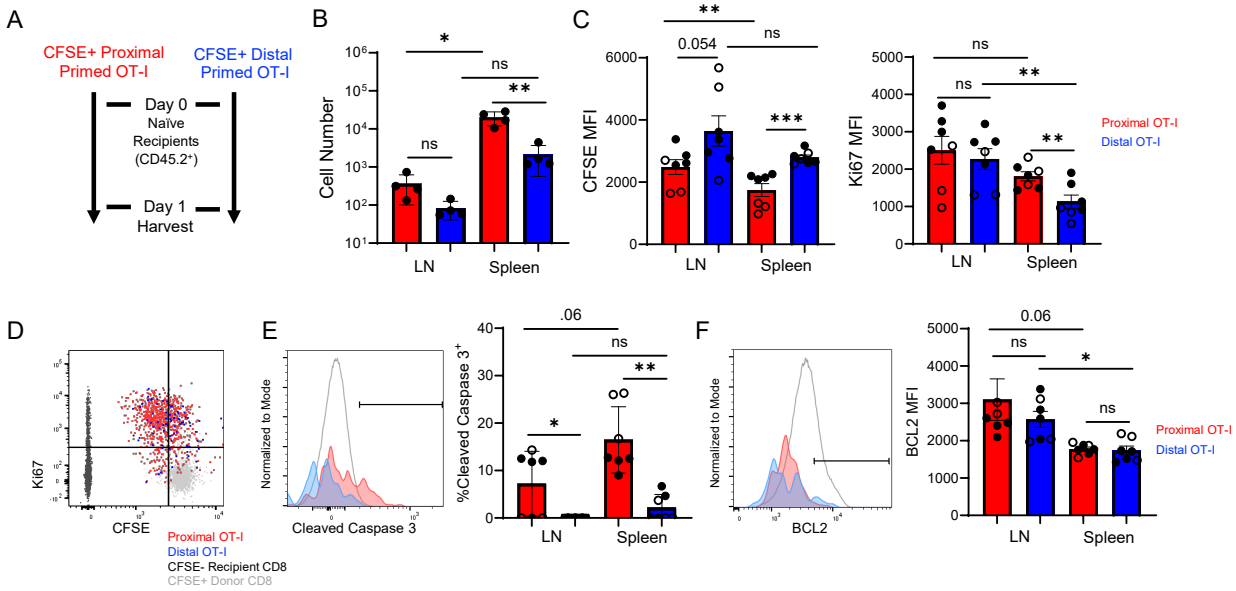

Figure 11. Distal IC-LN derived T cells have reduced immediate proliferation rate.

(A-C) 4 days post immunization of B6 mice transferred with OT-I T cells, proximal and distal IC-LNs were harvested into separate single cell suspensions, labeled with CFSE, and quantified. A total of 10^5 OT-I cells from either IC-LN type was re-transferred into separate cohorts of naïve B6 mice. 1 day later, spleen and pooled cutaneous lymph nodes from individual mice were analyzed by flow cytometry (n = 3 – 4, 2 experiments). (A) Schematic of experimental design. (B) Quantification of the total number of proximal and distal IC-LN derived OT-I T cells. (C) Quantification of CFSE gMFI and expression of Ki67 by the re-transferred OT-I T cells. (D) Representative flow plot of CFSE fluorescence and Ki67 expression by the re-transferred proximal and distal OT-I T cells, as well as by the endogenous polyclonal CFSE-labeled donor and unlabeled recipient CD45.2$^+$ CD8 T cells isolated from the spleen. (E) Representative plots and quantification of cleaved caspase 3 and F) BCL2 expression. All data are representative of at least two experiments with at least three mice per group in each experiment. Data from multiple pooled experiments are denoted by different symbols within the same group. Graphs show mean ± SD and were analyzed using paired Student's t test. ****P < 0.0001; ***P < 0.001; **P < 0.01; *P < 0.05; P > 0.05 not significant (ns).

4.2. REMOVAL OF STIMULATION PROMOTES SUPERIOR RECALL OF PROXIMAL IC-LN DERIVED T CELLS FOLLOWING RE-CHALLENGE

We next evaluated how T cells generated in different IC-LNs contribute to memory responses. For this, equal numbers of congenically disparate OT-I T cells ($CD45.1^+$ versus $CD45.1^+CD45.2^+$) primed in either proximal or distal IC-LNs were re-transferred together into naïve $CD45.2^+$ recipients. At memory timepoints (30-60 days post re-transfer), these mice were intravenously (i.v.) administered OVA plus CpG to induce recall responses (Fig. 12. A, naïve recipients). Analysis of lymphoid organs and lungs 3 days post recall demonstrated that both proximal and distal derived T cells underwent efficient expansion, albeit with a favoring of proximal-derived cells over their distal-derived counterparts (Fig. 12. B-E). These numerical differences were consistent with the early divergence in cellular recovery immediately post re-transfer (Fig. 12. B). Cells derived from both sources were indistinguishable by their phenotypic and functional properties (Fig. 12. F), indicating functionally equivalent recall ability. Of note, due to low recovery of re-transferred T cells without OVA recall, we were unable to compare the overall ability of cells from different sites to generate memory populations prior to recall. Regardless, our findings indicate that upon re-transfer into naïve recipients, proximal IC-LN cells have an enhanced ability to proliferate and to generate memory recall. Yet, T cells generated across the entire lymphatic chain contribute to the cumulative sum of memory responses.

4.3. DISTAL IC-LN DERIVED T CELLS HAVE SUPERIOR RECALL WHEN GIVEN CONTINUED STIMULATION FOLLOWING LYMPHATIC PRIMING

We also reasoned that normally, activated T cells may undergo additional cognate stimulation either in draining LNs or after trafficking to sites of inflammation, and this would be absent after re-transfer into naïve mice. We thus re-transferred equal number of proximal versus distal primed OT-I T cells into secondary recipients, which were also immunized in the footpad with OVA plus CpG at the time of transfer to provide an additional source of antigen and inflammation (Fig. 12. A, 2' immunized recipients). Examination of cellular recall at memory timepoints again demonstrated robust expansion of OT-I T cells derived from both proximal and distal IC-LNs (Fig. 12. D). However, unlike findings with T cells transferred into naïve mice, in 2' immunized recipients, T cells from distal IC-LNs exhibited numerically superior recall and dominated the response as compared to those derived from proximal IC-LNs, and this was observed across all examined organs (Fig. 12. B-E). Notably, we also observed phenotypic differences in recalled T cells from different sources, which were consistent with their phenotype at the time of initial re-transfer. A higher frequency of recalled cells derived from distal IC-LNs were $TCF1^{+}$ and expressed higher levels of CD62L, while conversely, more proximal IC-LN-derived T cells displayed enhanced effector cell properties, as characterized by increased T-BET and Granzyme B expression (Fig. 12. G). These data suggest that upon continued exposure to antigen and inflammation, T cells activated in distal IC-LNs have an advantage in their ability to generate memory recall responses, and that additional rounds of cognate stimulation post re-transfer elicit long-term imprinting of effector versus progenitor properties in the responding cells.

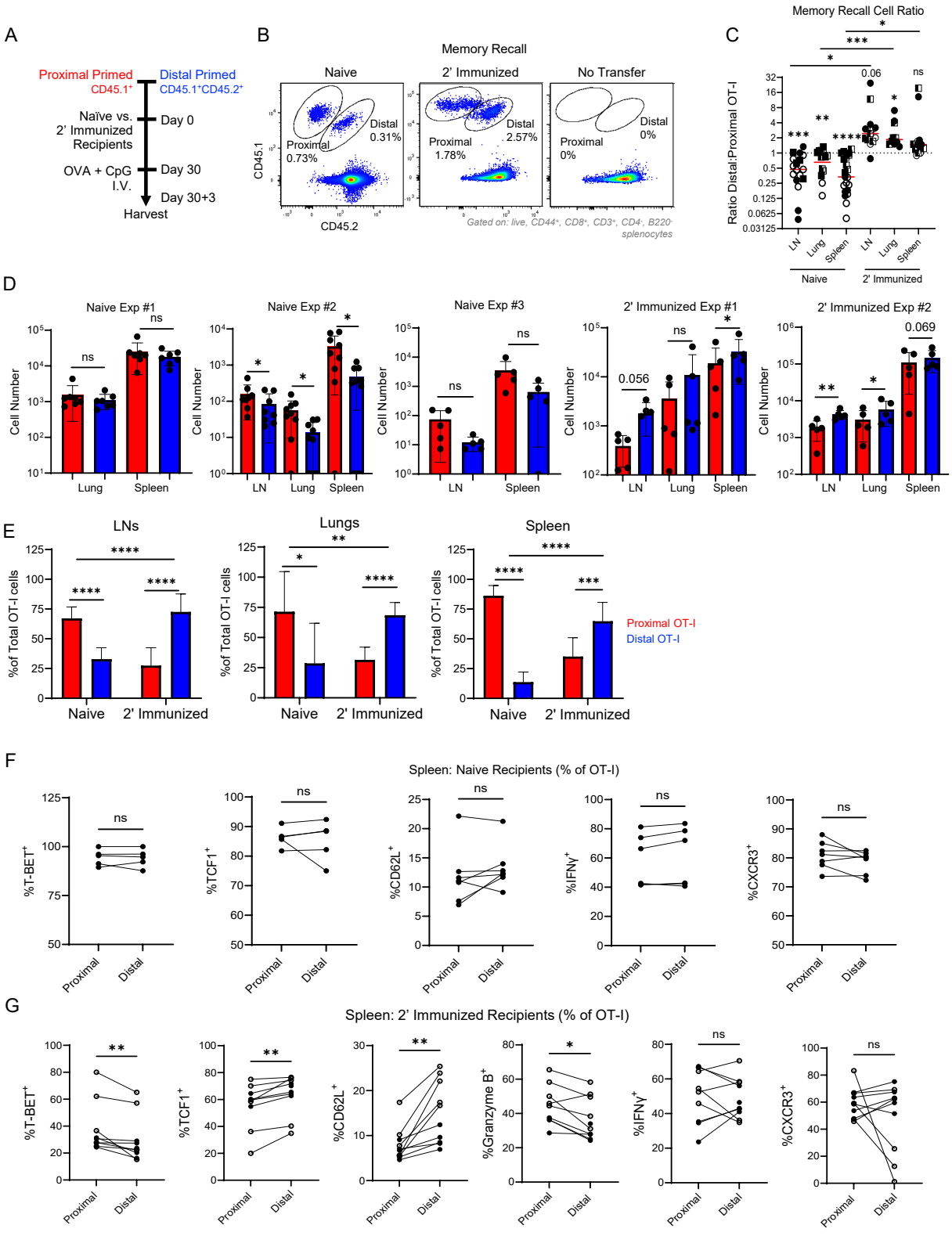

Figure 12. Proximal and distal IC-LNs generate distinct CD8 memory responses.

Congenically disparate ($CD45.1^+$ / $CD45.1^+.2^+$) OT-I T cells were primed in separate B6 recipients, isolated from proximal and distal IC-LNs, and then re-transferred at a 1:1 ratio into new $CD45.2^+$ B6 hosts, which were either untreated (Naïve) or immunized with OVA + CpG in the footpad at the time of re-transfer (2' Immunized). 30 days post re-transfer, mice were intravenously administered OVA + CpG to elicit recall. 3 days later, pooled LNs, spleen, and lung were harvested for analysis by flow cytometry (n = 5, 3 experiments). (A) Schematic of experimental design. (B) Representative flow plots of proximal and distal IC-LN derived OT-I cell T cells isolated from the spleen following recall. (C) Cellular ratios of distal to proximal IC-LN derived OT-I T cells. Dotted line represents the original 1:1 ratio at re-transfer. Dotted line represents the original 1:1 ratio at re-transfer. (D) OT-I T cell numbers from individual memory recall experiments in naïve and 2' immunized recipient mice. (E) Frequency of responding transferred OT-I T cells that are either of distal or proximal IC-LN origin. (F-G) Expression patterns of the indicated cell markers by OT-I T cells isolated from the spleen following recall in F) naïve or G) 2' immunized recipients. Data from multiple pooled experiments are denoted by different symbols within the same group. Graphs show mean ± SD and were analyzed using paired Student's t test for comparison within the same mice or unpaired for comparisons between mice. ****$P < 0.0001$; ***$P < 0.001$; **$P < 0.01$; *$P < 0.05$; $P > 0.05$ not significant (ns). Wilcoxon signed-ranked test was used to compare new ratios of distal to proximal cells to a hypothetical value of 1 (ratio at time of transfer).

4.4. PROXIMAL IC-LN-DERIVED T CELLS MAKE UP THE MAJORITY OF TUMOR INFILTRATING CD8 T CELLS AT EARLY TIMEPOINTS BUT UNDERGO ACCELERATED EXHAUSTION

Memory precursor T cells demonstrate superior persistence in response to chronic tumor antigens (Angelosanto et al., 2012). Given that T cells from distal IC-LNs exhibited enhanced memory capabilities after continued antigen exposure, we next hypothesized that these cells would also show greater persistence upon tumor challenge. To test this, we examined the responses of T cells

generated in different IC-LNs to chronic antigen exposure in the context of B16 melanoma tumors engineered to express OVA. Mice were transplanted with B16.OVA tumors, and 8-10 days later, once the tumors became palpable, they were co-injected with equal numbers (10^5) of congenically disparate distal and proximal IC-LN primed OT-I T cells (after 4 days of activation in their respective IC-LNs). Additionally, some mice were co-transplanted with both parental B16 and B16.OVA tumors on contralateral flanks, allowing us to assess the antigen dependence of T cell responses and trafficking in this system. Tumors and tumor draining LNs were harvested at various time points post re-transfer for analysis (Fig. 13. A). We observed markedly elevated numbers of OT-I T cells in the B16.OVA tumors and associated draining LNs as compared to the parental B16 tumors and LNs (Fig. 13. B), indicating a continued need for antigen for cellular retention and responses in both tissue types. Within the B16.OVA tumors, we observed an early numerical bias (1 day post transfer) for proximal IC-LN derived T cells (Fig. 13. C), consistent with the enhanced cycling rates and ability of effector cells to traffic to sites of inflammation. In contrast, T cells from both sources were equally represented in tumor draining LNs (Fig. 13. C), suggesting that T cells generated across the entire lymphatic chain can recirculate and contribute to additional responses in LNs.

Consistent with the early priming differences among the sites, tumor infiltrating T cells derived from proximal IC-LNs had significantly increased Granzyme B expression (Fig. 13. D), indicating increased effector function 1 day post transfer. Both cell populations were capable of producing IFNγ in the tumor following re-stimulation (Fig. 13. E). Notably, we also observed increased expression of the exhaustion marker, TIM3, on tumor-infiltrating proximal IC-LN derived T cells, while distal IC-LN derived T cells had a converse increase in Ly108 expression

(Fig. 13. F), indicating distinct rates of early exhaustion (Beltra et al., 2020). In contrast and consistent with prior literature (Connolly et al., 2021; Huang et al., 2022b; Prokhnevska et al., 2023; Rahim et al., 2023; Schenkel et al., 2021), in tumor draining LNs, the majority of T cells from both sources continued to express Ly108 and lacked TIM3 expression, as well as expressed Ki67 (Fig. 13. G-H), indicating ongoing proliferation and lack of exhaustion within lymphoid organs. Surprisingly, over time the numerical differences within the tumor diminished, and by day 11, both cellular sources were equivalently represented (Fig. 13. I-J). While both populations expanded from day 1 to day 11, the relative fold increase in cellularity was markedly greater for distal IC-LN derived T cells in the tumor compared to proximal IC-LN-derived T cells (78-fold versus 14-fold, respectively) (Fig. 13. K).

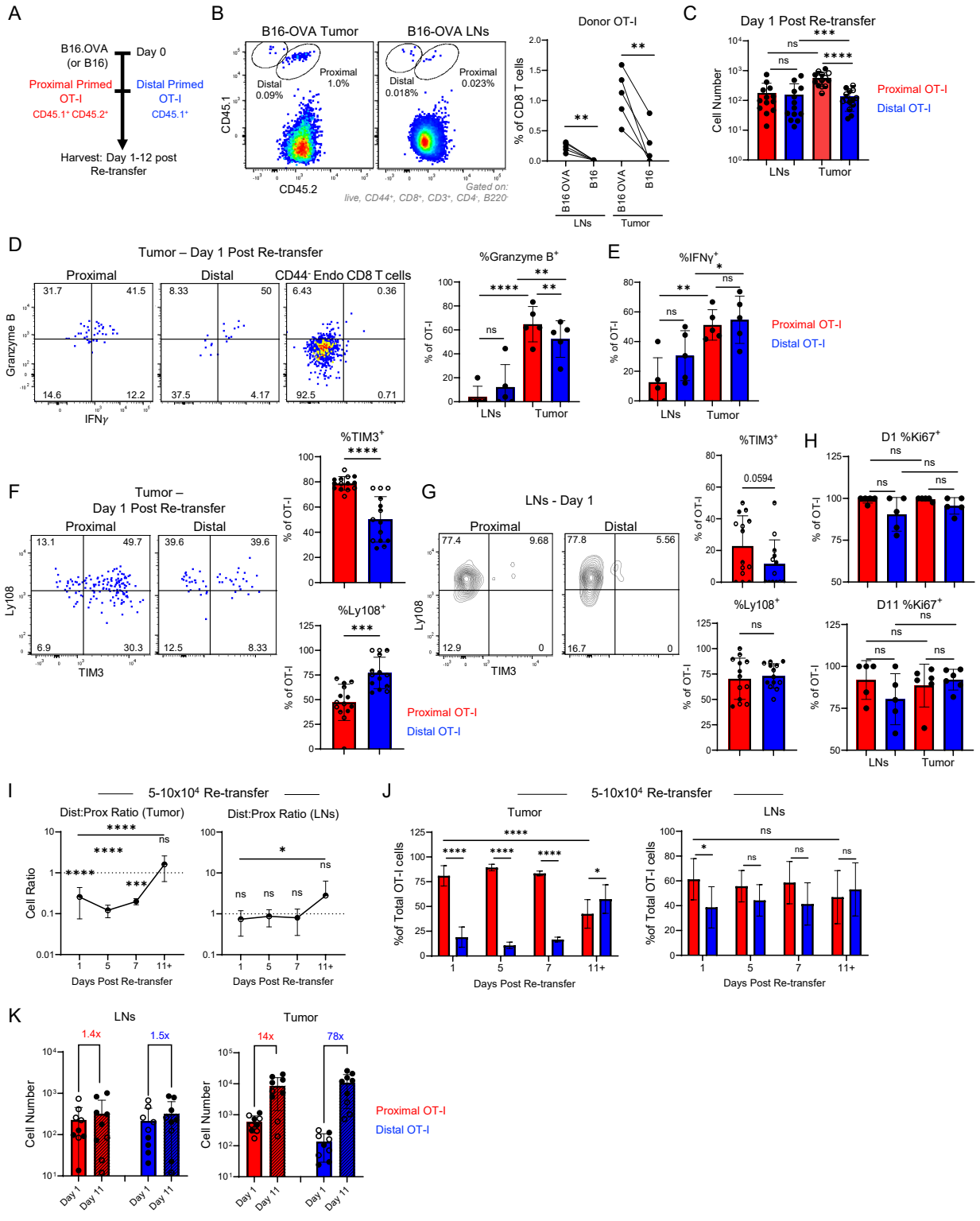

Figure 13. Proximal IC-LN CD8 T cells dominate the early tumor response but rapidly undergo exhaustion.

Congenically disparate ($CD45.1^+$ / $CD45.1^+.2^+$) OT-I T cells were primed in B6 recipients, isolated from proximal and distal IC-LNs, and quantified. 5-10x10^4 proximal and distal OT-I CD8 T cells each were re-transferred at a 1:1 ratio into new B16.OVA (or also B16 on contralateral side) tumor-bearing mice. Tumors and tumor draining LNs were harvested at the indicated time points post transfer (n = 4 – 5/group, 4 experiments). (A) Schematic of experimental design. (B) Representative flow plots demonstrating gating of the re-transferred OT-I T cells in B16-OVA tumors and pooled tumor draining dLNs (LNs). Quantification of the frequency of OT-I T cells 3 days post re-transfer into mice bearing both B16.OVA and B16 tumors on contralateral flanks. (C) Proximal and distal OT-I T cell numbers were quantified 1 day following re-transfer. (D-E) Representative plots and quantification of D) Granzyme B and E) IFNγ expression following *ex vivo* re-stimulation by the OT-I T cells relative to endogenous $CD44^-$ CD8 T cells. (F-G) Representative flow plots and quantification of TIM3 and Ly108 expression by F) tumor-infiltrating OT-I T cells and in the G) tumor draining LNs 1 day post re-transfer. (H) Quantification of Ki67 expression by the proximal and distal OT-I T cells 1 and 11 days post re-transfer. (I) Ratio of distal to proximal IC-LN derived OT-I T cells in B16.OVA tumors and tumor draining LNs across different time points. (J) Percent of total transferred OT-I CD8 T cells that are either of proximal or distal origin across different time points post re-transfer of 5-10x10^4 cells. (K) Fold expansion of proximal and distal OT-I T cells from day 1 to day 11 following re-transfer. Data from multiple pooled experiments are denoted by different symbols within the same group. Graphs show mean ± SD and were analyzed using paired Student's t test for comparison within the same mouse or un-paired between separate mice. ****$P < 0.0001$; ***$P < 0.001$; **$P < 0.01$; *$P < 0.05$; $P > 0.05$ not significant (ns). Wilcoxon signed-ranked test was used to compare new ratios of distal to proximal cells to a hypothetical value of 1 (ratio at time of transfer).

4.5. DISTAL IC-LN-DERIVED T CELLS HAVE PROLONGED PROLIFERATION POTENTIAL AND DISPLAY A T_{PEX} LIKE PHENOTYPE

Long-term advantage in expansion by distal IC-LNs could have arisen due to the enhanced ability of these cells to form T_{PEX} cells, which have been implicated as a self-renewing population that fuels long-term T cell responses under chronic settings (Im et al., 2016; Siddiqui et al., 2019; Utzschneider et al., 2016). Consistent with this idea, at timepoints preceding the numerical convergence of the populations, tumor infiltrating T cells demonstrated non-equivalent expression of progenitor versus exhaustion markers, with a greater fraction of T cells from distal IC-LNs co-expressing TCF1 and Ly108 (Fig. 14. A), indicating preferential ability to generate T_{PEX} cells. Consistent with day 1 data, both populations in the tumor draining LN continued to co-express TCF1 and Ly108 at these later timepoints (Fig. 14. B), indicating the retention of a T_{PEX} phenotype in lymphoid organs. Conversely, in the tumor a higher frequency of proximal IC-LN derived T cells lacked TCF1 expression while expressing more Granzyme B. Indeed, analysis of total cellularity with respect to phenotype showed that at these timepoints, numerical differences among populations were mainly driven by increased representation of T_{EX} cells derived from proximal IC-LNs, while total T_{PEX} were not significantly different (Fig. 14. C).

Precursor frequency and magnitude of expansion can alter the nature and kinetics of immune responses (Hataye et al., 2006; Marzo et al., 2005; Obar et al., 2008). We thus re-transferred lower numbers of OT-I CD8 T cells (5-10x10^3) into the B16.OVA transplanted recipients and analyzed the relative composition and properties of distal versus proximal IC-LN primed T cells over time. As above, early responses within tumors were numerically dominated by proximally-derived OT-I CD8 T cells, while draining LNs were populated by populations from both sources, with a modest favoring of distally-derived cells (Fig. 14. D-E). As in the high-transfer experiments, we observed that over time the differences within the tumor normalized, albeit at a

faster rate, as by day 9, both cellular sources were equivalently represented within the tumors, while distal IC-LN derived cells continued to dominate the tumor draining LNs (Fig. 14. D-E). We again noted a persistent reduction in TIM3 expression on distal IC-LN-derived tumor infiltrating T cells (Fig. 14. F), indicating reduced T cell exhaustion. Consistent with this, while both populations expressed PD1, we noticed an enrichment in $PD1^{+}TCF1^{+}$ T_{PEX} cells in the distal IC-LN derived population 7 days post re-transfer (Fig. 14. G). Together, these data suggest that while the very early intra-tumoral responses are dominated by proximal IC-LN derived effector CD8 T cells, these cells undergo rapid exhaustion and lose their numerical advantage in the tumor over-time. In contrast, distal IC-LN derived T cells have an enhanced propensity to generate T_{PEX} cells, seed lymphoid organs, and thus have greater long-term expansion potential.

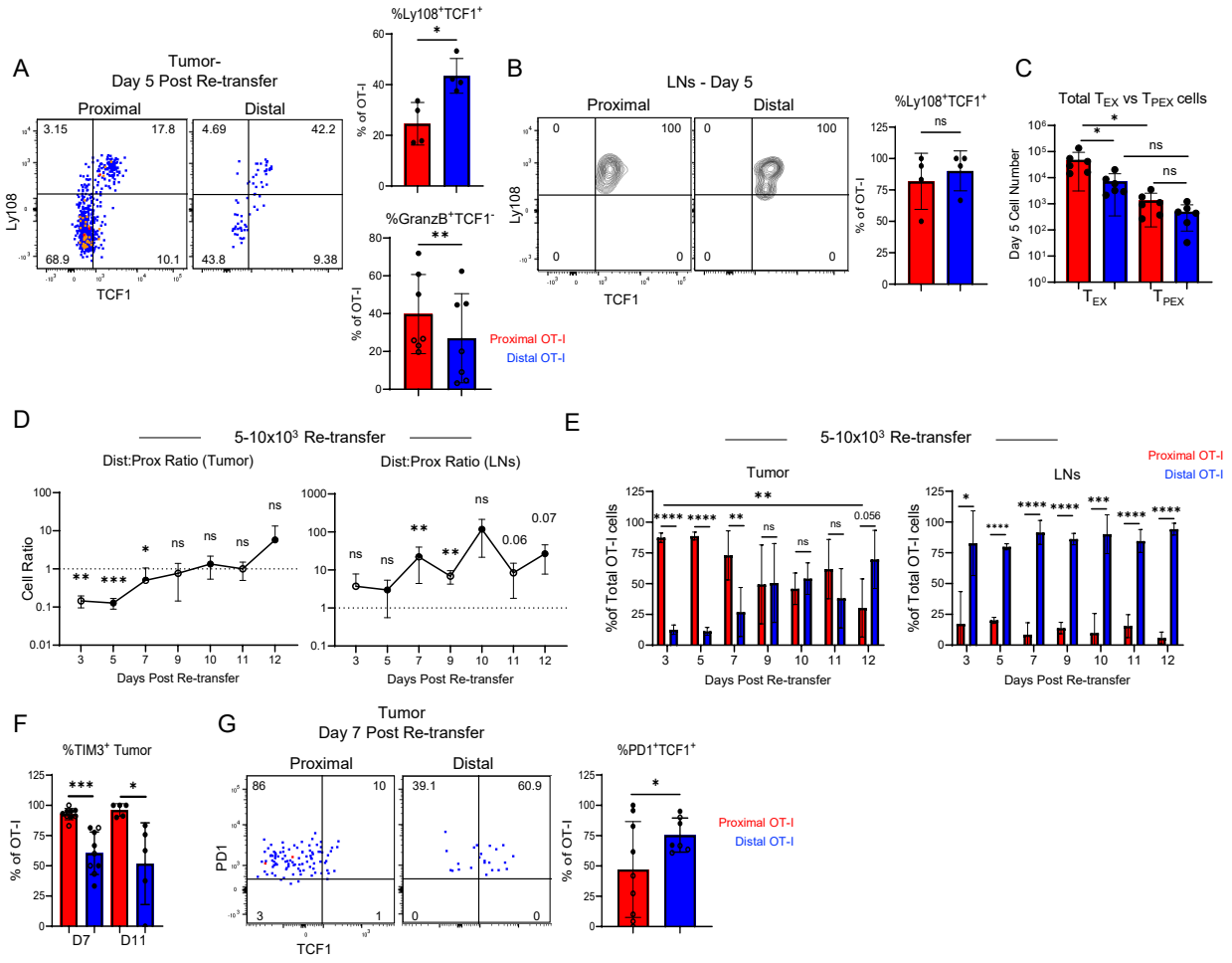

Figure 14. Distal IC-LN CD8 T cells show prolonged proliferation and T_{PEX} phenotype.

(A-C) Congenically disparate ($CD45.1^+$ / $CD45.1^+.2^+$) OT-I T cells were primed in B6 recipients, isolated from proximal and distal IC-LNs, and quantified. 5-10x10^4 proximal and distal OT-I CD8 T cells each were re-transferred at a 1:1 ratio into new B16.OVA (or also B16 on contralateral side) tumor-bearing mice. Tumors and tumor draining LNs were harvested at the indicated time points post transfer (n = 3 – 5/group, 2 experiments). (A-B) Expression of Ly108, Granzyme B, and TCF1 by OT-I T cells in the A) tumor and B) tumor draining LNs 5 days post re-transfer. (C) Total number of T_{EX} ($GranzB^+TCF1^-$) and T_{PEX} ($Ly108^+TCF1^+$) cells in the tumors day 5 post re-transfer of 5-10x10^4 cells. (D) Ratio of distal to proximal IC-LN derived OT-I T cells in B16.OVA tumors and tumor draining LNs at indicated timepoints post re-transfer of 5-10x10^3 OT-I T cells from each source. (E) Percent of total transferred OT-I CD8 cells that

are either of proximal or distal origin across different time points post re-transfer of 5-10x10^3 cells. (F) Expression of TIM3 by proximal and distal OT-I T cells 7 and 11 days post re-transfer. (G) Representative plots and quantification of PD1 and TCF1 expression by OT-I T cells at the indicated timepoint.

4.6. DISTAL IC-LN DERIVED T CELLS PROLIFERATE MORE THAN PROXIMAL IN RESPONSE TO CHECKPOINT THERAPY

T_{PEX} cells are thought to be the target of immune checkpoint inhibitors, such as anti-PDL1/-PD1 antibody treatments. Therefore, we examined whether CD8 T cells derived from proximal versus distal IC-LNs have differential abilities to respond to checkpoint blockade therapy. For this, 10 days after T cell re-transfer into B16.OVA-bearing mice, a time point associated with equilibration of T cell responses within tumors, mice were treated with anti-PDL1 or isotype control antibody. Responses in tumors and draining LNs were examined 4 days after initiation of treatment (Fig. 15. A). PDL1 blockade resulted in increased numbers of endogenous CD8 T cells in the tumor (Fig. 15. B), indicating enhancement of anti-tumor responses. Notably, checkpoint blockade also induced a significant and consistent enrichment of distal-primed OT-I T cells relative to proximal-derived cells within the tumor, and this was not seen after isotype control treatment (Fig. 15. C, E). Increased representation of distally derived T cells was also observed in tumor draining LNs, albeit there was no obvious effect of anti-PDL1 treatment on further cellularity enhancement (Fig. 15. D-E). Phenotypic characterization demonstrated that the majority of tumor infiltrating cells from both sources expressed high levels of TIM3 and PD1, as well as were Ly108 negative (Fig. 15. F). In contrast to tumors, both distal and proximal T cells located in tumor draining LNs continued to express Ly108 and PD1, indicating maintenance of the T_{PEX} status irrespective of

treatment. As before, within the tumor, we continued to observe a numerical dominance of T_{PEX} cells derived from distal IC-LNs (Fig. 15. G), indicating enhanced long-term persistence. Importantly, checkpoint blockade therapy selectively increased the number of distal IC-LN derived $TIM3^{+}Ly108^{-}$ T_{EX} cells in the tumor, and this was not seen for T cells derived from proximal IC-LNs (Fig. 15. H). This suggested preferential expansion and generation of T_{EX} cells following checkpoint blockade therapy by distal IC-LN T cells, as well as absence of such responses by proximal IC-LN derived cells. Together, these data indicate that anti-tumor response outputs are provided by T cells derived from across the entire chain of LNs. However, over time, there is a strong favoring for cells generated in distal IC-LNs due to their enhanced ability to seed lymphoid organs, and to generate T_{PEX} cells capable of long-term persistence and enhanced proliferation following checkpoint blockade therapy.

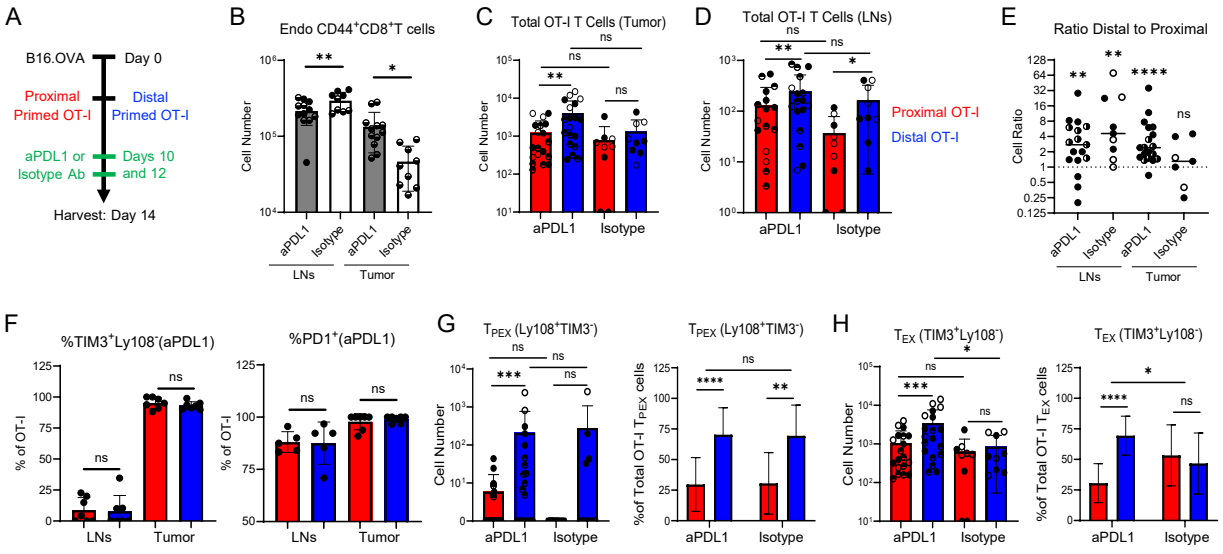

Figure 15. Distal IC-LN CD8 T cells respond better to checkpoint blockade therapy.

Following re-transfer of 5-10x10^{3} congenically disparate proximal and distal IC-LN derived OT-I T cells into B16.OVA bearing mice, recipients were treated with anti-PDL1 or IgG isotype control antibody at day 10 and day 12. Tumors and LNs were harvested on day 14 for analysis by

flow cytometry (n = 4 – 7/group, 3 experiments). (A) Schematic of experimental design. (B) Quantification of the total $CD44^+$ endogenous CD8 T cells in the tumor and tumor draining LN following treatment with anti-PDL1 or isotype control antibody. (C-D) Quantification of the total proximal or distal derived OT-I T cell numbers in the C) tumor and D) tumor dLNs following treatment. (E) Quantification of the ratio of distal to proximal IC-LN derived OT-I T cells following treatment. (F) Frequency of cells expressing the indicated markers in the tumor and tumor draining LNs following treatment. (G-H) Frequency and total cell numbers of responding proximal or distal derived OT-I T cells in the tumor that are of a G) T_{PEX} ($Ly108^+TIM3^-$) or H) T_{EX} ($TIM3^+Ly108^-$) phenotype. All data are representative of at least two experiments with at least three mice per group in each experiment. Data from multiple pooled experiments are denoted by different symbols within the same group. Graphs show mean ± SD and were analyzed using paired Student's t test for comparison within the same mouse or un-paired between separate mice. For anti-PDL1 treated versus isotype control samples, non-parametric unpaired T test was used. ****$P < 0.0001$; ***$P < 0.001$; **$P < 0.01$; *$P < 0.05$; $P > 0.05$ not significant (ns). Wilcoxon signed-ranked test was used to compare new ratios of distal to proximal cells to a hypothetical value of 1 (ratio at time of transfer).

Chapter 5. DISCUSSION

In the current study, we observed differences in antigen uptake, DC maturation, inflammatory chemokine production, monocyte recruitment, and IL-12 production by both DCs and monocytes across the lymphatic chain. We predict that the combination of all these factors contribute to differential T cell responses observed across the chain, therefore the lymphatic spread of VDMs across IC-LNs facilitates the generation of a heterogenous T cell response (Fig. 16). Our overall findings support the notion that the enhanced generation of effector and effector memory precursor T cell responses in proximal IC-LNs results from increased antigen availability and inflammation (Huang et al., 2022a). Conversely, reduced abundance of these signals in distal IC-LNs is

associated with minimal effector differentiation and the generation of central memory precursor cells (Kaech and Cui, 2012). Of note, the use of FTY720 to block T cell egress does not rule out the possibility of intra-lymphatic trafficking of effector T cells during priming. It is possible that effector T cells migrate from proximal to distal IC-LNs and receive additional signals there or influence local responses. Similarly, it remains to be determined whether cytokines or other signals are transmitted across lymphatic chains during the generation of immune responses.

Notably, our fate-tracking studies using cell re-transfer demonstrated that both sites could produce functional memory recall, with an advantage for proximal IC-LN derived cells if the cells are re-transferred into unstimulated naïve recipient mice. The generation of functional memory, even with markedly enhanced effector responses in proximal IC-LNs, indicates retention of plasticity by the early differentiated effector cells upon cessation of stimulation (Abadie et al., 2024; Chu et a., 2025; Herndler-Brandstetter et al., 2018; McManus et al., 2025; Soerens et al., 2023; Youngblood et al., 2017). The numerical dominance of proximal IC-LN-derived cells during recall appears to result from increased rates of proliferation upon re-transfer into naïve recipients. These data are directly concordant with recent evidence that cells with optimal recall capacity, such as central memory precursor cells, cycle at slower rates and undergo fewer rounds of proliferation compared to effector or effector memory precursor populations (Bresser et al., 2022; Kretschmer et al., 2020).

In contrast to unstimulated naïve recipient mice, we found preferential induction of memory recall by distal IC-LN derived T cells upon re-vaccination and continued exposure to antigen and inflammation after re-transfer. We also observed long-term imprinting of the effector

program by the proximal IC-LN-derived cells after recall, suggesting establishment of heterogeneity in the memory compartment based on the initial site of priming. These findings are consistent with evidence that prolonged antigen stimulation is necessary to foster the formation of superior memory T cells (Henrickson et al., 2013; Kretschmer et al., 2020; Shaulov and Murali-Krishna, 2008), and that continued sensing of inflammatory signals in inflamed sites drives terminal effector differentiation by T cells (Bangs et al., 2022; Chow et al., 2019; Duckworth et al., 2021; Goldberg et al., 2018; Groom et al., 2012; Hu et al., 2011; Kurachi et al., 2011; Ozga et al., 2022). Additional divergence of responses could result from non-equivalent positioning of T cells in lymphoid and non-lymphoid organs, promoting distinct secondary interactions with APCs following re-transfer. It is critical to note that our studies conducted a head-to-head comparison of cells generated within a single distal IC-LN versus those derived from proximal IC-LNs. Yet, we also observed abundant activation of T cells across multiple distal IC-LNs, including iliac LNs, which displayed additional alterations in homing molecule expression on responding T cells. It will thus be important to unravel how cells generated across the entire chain of LNs contribute to the cumulative sum of adaptive responses and memory recall.

Finally, we find differential contributions of T cells derived from both proximal and distal IC-LNs to the adaptive response to tumors. Our data demonstrate that while proximal IC-LN-derived CD8 T cells exhibit enhanced early trafficking abilities and effector functions within tumors, they are also more prone to exhaustion and their numerical advantage dissipates over time. In contrast, higher frequencies of distal IC-LN-derived T cells maintain a T_{PEX} phenotype in tumor tissues, outnumber proximal-derived T cells in tumor-draining LNs, and generate enhanced responses following checkpoint blockade therapy. Notably, we also found that while there is

preferential propensity of distally derived T cells to generate T_{PEX}, proximal IC-LN derived T_{PEX} numerically are equivalent to or can even dominate at early-intermediate time points following retransfer, at least as defined by expression of canonical markers TCF1, Ly108, and lacking expression of TIM3. Yet, these proximal-derived T_{PEX} failed to survive and contribute to long-lived responses following anti-PDL1 treatment. These data suggest that additional layers of heterogeneity likely exist within the T_{PEX} population that determine its long-term responses, and these may be due to either intrinsic properties or localization differences and extrinsic effects of the environment. While we demonstrate non-equivalent T cell longevity and reactivation following checkpoint blockade therapy, our study did not directly assess whether T cells from different IC-LNs confer differential protective effects against cancer or other diseases. Future studies are needed to elucidate the contributions of distinct tissue sources to durable protective immunity, as well as to understand how to better manipulate this axis with rational vaccine design.

Why does the formation of T_{PEX}-like cells from distally IC-LN-derived CD8 T cells matter? Tumor-infiltrating CD8 T cells are an established correlate of improved prognosis for many cancer types, particularly those expressing immunogenic tumor-associated antigens (Combes et al., 2022; Galon et al., 2006; Waldman et al., 2020). Current models suggest that checkpoint blockade immunotherapies enhance CD8 T cell responses primarily by targeting T_{PEX} cells, which then proliferate to generate effector and eventually exhausted T cells, resulting in waves of anti-tumor protection (Huang et al., 2022b; Siddiqui et al., 2019). These responses can originate from either reactivation of cells within the tumor microenvironment or engagement of T_{PEX} cells in tumor-draining LNs (Connolly et al., 2021; Di Pilato et al., 2021; Garris et al., 2022; Huang et al., 2022b; Li et al., 2022; Meiser et al., 2023; Prokhnevska et al., 2023; Schenkel et al., 2021; Siddiqui et al.,

2019; Steele et al., 2023; Stoltzfus et al., 2021), and it is likely that the enhanced longevity of distal IC-LN-derived T cell anti-tumor responses is afforded by processes in both sites.

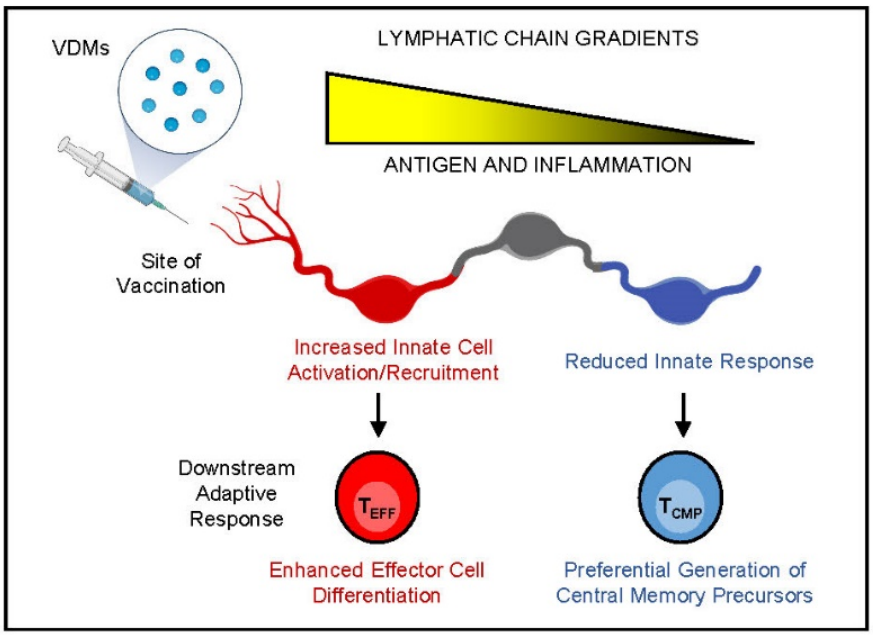

Figure 16. Proposed model for how lymphatic chains contribute to the heterogenous T cell response.

Chapter 6. FUTURE DIRECTIONS

Using lymphatic tracers and fluorescently labeled proteins, we observed efficient spread of antigens across LN chains but not to distal organs. Similar lymphatic dispersal has been documented with various vaccine formulations (Irvine et al., 2020), including mRNA lipid nanoparticle vaccines, in both mice and non-human primates (Hassett et al., 2024; Havenar-Daughton et al., 2019; Martin et al., 2021; Smedley et al., 2014). VDMs drainage across IC-LNs results in the induction of robust T cell responses and the generation of heterogeneity across LN chains in response to soluble, particulate, and oil-in-water emulsion formulations, suggesting that

lymphatic chain-based priming is a general feature of most subunit vaccines. In contrast, the rules governing adaptive response heterogeneity with live attenuated formulations, especially when administered to mucosal tissues, likely differ, as these more closely mimic natural infections including the complexity of tropism and replication rates of different vectors (Pulendran et al., 2021; Zhao et al., 2023). Previous engineering efforts aimed at enhancing vaccine targeting of draining LNs resulted in marked improvements in T cell responses while also reducing systemic inflammation (Liu et al., 2014; Lynn et al., 2015). Similarly, increasing the duration of antigen availability in draining LNs with use of engineered bioparticles has been shown to enhance humoral responses (Lee et al., 2022; Tam et al., 2016). Conversely, excessive innate inflammatory responses triggered by certain formulations, such as complete Freund's adjuvant, can impede lymphatic dispersal and suppress the adaptive immune response at distal LNs (Yang and Unanue, 2013). Therefore, formulation design that considers both bio-dispersal and antigen availability across IC-LNs, as well as the capacity to induce localized inflammation, will facilitate a more rational approach to eliciting adaptive responses of desired magnitude and quality. It remains to be investigated whether these same formulations limit the generation of memory T cell responses in distal IC-LNs, as well as influence B cell response heterogeneity across the lymphatic chain.

The route of vaccine administration is also known to play a critical role in shaping T cell responses. Our findings demonstrate that both cutaneous and intramuscular delivery facilitate lymphatic dispersal and generation of effector T cell heterogeneity across LN chains. However, the innate cells residing in distinct peripheral tissues differ (Irvine et al., 2020), potentially influencing the specific inflammatory signals produced both at the vaccination site and within the LNs. These differences may also impact the composition and activation states of antigen-

presenting cells that drive T cell responses (Brown et al., 2023; Cruz de Casas et al., 2024; Esterházy et al., 2019; Lyons-Cohen et al., 2024). Similarly, previous studies have shown that administering the same vaccine via intravenous versus subcutaneous routes results in distinct memory and effector T cell responses (Baharom et al., 2021). Thus, while we propose that lymphatic gradients broadly regulate cellular response heterogeneity in subunit vaccine-driven immunity, the specific immune outcomes will depend on the adjuvants and the route of administration (Irvine et al., 2020; Zhao et al., 2023).

Past studies have demonstrated that LN-resident DCs dominantly shape T cell activation during vaccination (Gerner et al., 2015; Gerner et al., 2017; Leal et al., 2021), indicating that inflammatory responses initiated by LN-resident innate cells upon sensing draining VDMs are sufficient for programming adaptive immunity. Nevertheless, migratory DCs do contribute to prolonged cellular responses and aid in programming T follicular helper cells, while retaining characteristics from their tissues of origin (Gerner et al., 2017; Krishnaswamy et al., 2017; Li et al., 2016; Lyons-Cohen et al., 2024). Our study did not assess the relative contributions of resident versus migratory DC subsets to T cell responses across the lymphatic chain. Notably, the prevailing paradigm suggests that migratory DCs primarily deliver antigens to the most proximal draining LNs (Braun et al., 2011), suggesting their impact may be limited in more distal IC-LNs. However, during influenza infection, lung migratory DCs have been reported to contribute to the generation of T cell response heterogeneity in both the draining mediastinal LNs and the distal spleen (Jenkins et al., 2021). This implies that continued migration of DCs via the lymphatics to downstream IC-LNs may be feasible and warrants further exploration. Furthermore, we observed antigen uptake by migratory DCs across the lymphatic chain within two hours of immunization. Given that

migration of DCs from the peripheral immunization site is unlikely within such a short time frame, this suggests that migratory DCs already present in the LNs due to homeostatic activation continue to capture antigen (Drutman et al., 2010). These findings highlight the need for future research to elucidate the interplay between lymphatic drainage and the role of distinct antigen-presenting populations in T cell priming.

In addition to vaccination settings, it will be interesting to examine whether heterogeneity in T cell responses across the lymphatic chain also occurs during natural (non-vaccination induced) immune responses to tumor development, either due to differences in antigen presentation or preferential tumor cell metastasis to proximal versus distal IC-LNs. Of note, most tumors lack the inflammatory properties necessary to drive substantial effector differentiation in draining LNs, an event that has been recently shown to occur directly within the tumor tissue (Prokhnevska et al., 2023). Along similar lines, it will be important to investigate how lymphatic chains contribute to effector differentiation following microbial infections.

Chapter 7. SIGNIFICANCE

Extensive evidence suggests that the overall strength and duration of stimulation, driven by the combined action of TCR and cytokine receptor signaling, dictate the diversification of T cell fates, particularly the formation of effector and memory T cells (Chang et al., 2014; Kaech and Cui, 2012; Shakiba et al., 2022). Our data introduce a critical spatial aspect to this signal strength model, demonstrating the establishment of concentration gradients of antigens and inflammatory signals across interconnected chains of LNs during vaccination which results in divergent T cell priming.

While all involved sites induce robust CD4 and CD8 T cell activation and memory cell formation, responses generated within individual IC-LNs are not equivalent in eliciting T cell effector differentiation and generating long-lived responses in the context of chronic antigen exposure, such as during cancer. Thus, our findings suggest that the magnitude and heterogeneity of adaptive immune responses induced by vaccines are spatially encoded through the biodistribution of VDMs across lymphatic chains. Notably, humans possess a significantly greater degree of LN interconnectedness compared to rodents, with 400–600 LNs in adults, most of which are organized in chains (Irvine et al., 2020; Oliver et al., 2020). This indicates that there's a higher likelihood of lymphatic gradients and LN chains generating immune response heterogeneity following vaccination in humans. Therefore, formulation design that considers both bio-dispersal and antigen availability across IC-LNs, as well as the capacity to induce localized inflammation, will facilitate a more rational approach to eliciting adaptive responses of desired magnitude and quality.

Our study used tumor models to examine functional differences between proximal and distal IC-LN derived T cells following vaccination. Such responses would be observed in tumor vaccination settings, such as those intending to elicit or amplify pre-existing CD8 T cell responses (Lin et al., 2022; Zhou et al., 2023). In fact, similar to the model utilized in this study, recombinant protein vaccines formulated with CpG agonist have been used in patients to prime cytotoxic CD8 T cells (Karbach et al., 2011). It stands to reason that in these contexts, distinct T cell populations generated across the lymphatic chain during vaccination provide non-equivalent modes of anti-tumor activity, and that the collective response from multiple IC-LNs leads to optimal immune protection. Our findings suggest that it may be crucial to design tumor vaccines that enhance VDM drainage across lymphatic chains to promote the generation of less-differentiated CD8 T cells with

prolonged tumor protection, particularly when coupled with additional checkpoint blockade immunotherapy.

Understanding the principles governing the heterogeneity and magnitude of adaptive responses generated by vaccines has long been a significant area of research. Our work lays the groundwork for understanding how vaccine biodistribution across lymphatic chains influences the magnitude and heterogeneity of adaptive T cell responses, thereby enabling the design of novel formulations for optimal immunological protection. Collectively, our findings indicate that the biodistribution of antigen and agonists following vaccination, governed by the fundamental rules of lymphatic physiology, generates information-rich gradients across the lymphatic chains. These gradients dictate the cumulative magnitude of cellular immunity and influence T cell response heterogeneity in a spatially encoded manner. These insights not only enhance our understanding of how T cell heterogeneity is established *in vivo* but also provide critical information for vaccine design aimed at achieving desired immunological responses.

Chapter 8. MATERIAL AND METHODS

8.1 MICE

6- to 8-week-old C57BL/6 (B6) were purchased from the Jackson Laboratory (Bar Harbor, ME, USA). B6.Cg-Tg(TcraTcrb)425Cbn/J (OT-II) and C57BL/6-Tg(TcraTcrb)1100Mjb/J (OT-I) were crossed to B6.SJL-*Ptprc*^{a} *Pepc*^{b}/BoyJ (CD45.1^{+} B6) mice (Charles Rivers Laboratory, Wilmington, MA, USA), and bred on site. 6- to 10-week-old male and female mice were kept in

specific pathogen–free conditions at an Association for Assessment and Accreditation of Laboratory Animal Care–accredited animal facility at the University of Washington, South Lake Union campus. All procedures were approved by the University of Washington Institutional Animal Care and Use Committee.

8.2 IMMUNIZATIONS AND FINGOLIMOD TREATMENT

The following adjuvants and amounts per immunization site were used: 20µg of CpG ODN 1668 (AdipoGen), Alhydrogel ("Alum") (Invivogen) mixed with 10 µg LPS (Sigma) diluted 1:1 with PBS, Room temperature (RT) AddaVax (Invivogen) was diluted 1:1 with PBS, and 10µg Endotoxin-free Ovalbumin ("OVA") (Invivogen). In some studies, a dose of 50µg OVA was given per injection. For antigen drainage studies, 10µg of OVA-AF488 (Thermo Fisher) plus 20µg of CpG injected subcutaneously (s.c.) in the hind footpad. Evans Blue (Sigma) was diluted 5:100 in PBS and injected into the hind footpad. A total volume of 20 µl was used for all footpad and intramuscular immunizations. To block T cell egress mice were treated with sphingosine-1-phosphate (S1P) receptor agonist FTY720 phosphate (Cayman Bio) following immunization at a concentration of 5 μg FTY720 per gram of mouse weight.

8.3 FLOW CYTOMETRY

For myeloid cell analysis, LN tissues were mechanically disrupted and subject to digestion in PBS with 10% fetal bovine serum (FBS) with DNase I (100µg/mL; Sigma), Dispase II (800µg/mL; Sigma), and Collagenase P (200µg/mL; Sigma) at 37°C shaking at 150rpm for 30 minutes with

periodic manual disruption. Flow cytometric studies of T cells in lymph nodes did not use enzymatic digestion. Lung and Tumor tissue was digested in complete RPMI with Liberase (70μg/mL; Roche) and DNase (100μg/mL; Sigma) and tissue was dissociated on the gentleMACS Dissociator (Miltenyi Biotec) as previously described (Hondowicz et al., 2016). Cell staining was conducted in the presence of Fc Block (2.4G2, Tonbo Biosciences) at 4°C for 30 minutes for all surface markers. Intracellular staining was performed for 45 minutes at 4°C after fixation with the FOXP3 Fix/perm kit (Invitrogen). In some studies, an addition permeabilization step was performed in 90% ice-cold methanol prior to intracellular staining. Tetramer staining was performed either at 4°C for 30 mins or at RT for 1 hr. H2Kb-SIINEKL Class-I Tetramer was kindly provided by Dr. Andrew Oberst (University of Washington). Flow cytometry data was acquired through the University of Washington, Cell Analysis Facility Shared Resource Lab, using the BD LSR II or BD Symphony A3 cytometer (NIH award 1S10OD024979-01A1). Data was analyzed using FlowJo software.

8.4 CONFOCAL MICROSCOPY AND HISTOCYTOMETRY

For confocal imaging, fixed LN tissue sections were imaged as previously described using a Leica SP8 microscope (Gerner et al., 2012). Briefly, isolated LN tissues were fixed using BD Cytofix (BD Biosciences) diluted 1:3 in PBS for 20–24 hours at 4°C then dehydrated with 30% sucrose solution for 24–48 hours at 4°C. LNs were then embedded in an OCT compound (Tissue-Tek) and stored at −20°C. Histocytometry and Cytomap analysis was performed as previously described (Gerner et al., 2012; Leal et al., 2021; Stoltzfus et al., 2020), with some modifications. Myeloid and T cell isosurface three-dimensional (3D) objects were generated in Imaris, and object statistics

were then exported to FlowJo software for gating and phenotypic characterization. For analysis of myeloid cells, a combinatorial myeloid channel was created by adding normalized signals for CD11c and SIRP-α using the Imaris XT channel arithmetic module, and this sum myeloid channel was used for myeloid isosurface object creation. For T cells, an activated T cell channel was created on IRF4, and then further gated on the congenic CD45.1 signal for OT-I analysis. Spatial correlation analysis was performed in CytoMAP (Stoltzfus et al., 2020). In brief, the position of all myeloid and T cell objects within LNs was used for virtual raster scanning with 50-µm radius neighborhoods. The Pearson correlation coefficient was calculated for the number of cells of different cell types within these neighborhoods.

8.5 CELL TRANSFERS

For adoptive transfers, naïve CD45.1$^+$ or CD45.1$^+$CD45.2$^+$ OT-I T cells, and naïve CD45.1$^+$ OT-II cells were isolated from LNs and spleens using either the naïve CD8$^+$ or CD4$^+$ T cell isolation kits (Miltenyi Biotec), respectively. Average purity of OT-I and OT-II cells was about 90 and 75%, respectively. 5x10^5 (unless otherwise noted) naïve cells were transferred into hosts intravenously via retro-orbital injection 1-3 days prior to immunization. For re-transfers, either Popliteal or Inguinal LNs from immunized primary OT-I recipients were harvested, pooled separately, and processed into single cell suspensions. Samples were stained for CD45.1, CD44, CD8, CD25, CD62L and CXCR3 to confirm differences in effector differentiation and to measure the frequency of OT-I cells. Equal numbers of congenically distinct pairs of 10^4-10^5 (as noted) proximal and distal IC-LN-derived OT-I cells were then intravenously re-transferred into CD45.2 C57BL/6 secondary recipient mice.

8.6 B16 MELANOMAS AND CHECKPOINT BLOCKADE THERAPY

7- to 10-week-old male B6 mice were s.c. injected with $5x10^5$ B16.F10 or B16.F10.OVA.mCherry cell line resuspended in 1x Phosphate Buffered Saline (PBS,100 μl) with growth factor reduced Matrigel (Corning,354230) (50 μl) in a total volume of 150 μl in the right flank. Mice were harvested 20-24 days after tumor injection for flow cytometry. For checkpoint blockade immunotherapy, randomized mice (similar average tumor volume among groups) were treated twice (every other day) with 200 μg of either anti-PDL1 (Bio X Cell) or isotype control antibody intraperitoneally (i.p.) starting day 10 post T cell re-transfer.

8.7 STATISTICS

Statistical analysis was performed using GraphPad Prism software. The statistical significance of differences in mean values between two groups was analyzed by a two-tailed unpaired student's t test with Welch's correction. Paired t tests were performed when comparing IC-LN responses across a single lymphatic chain in experimental mice. In bar graphs for all figures, data is shown as mean with standard deviation. ****$p<0.0001$; ***$p<0.001$; **$p<0.01$; *$p<0.05$; $p>0.05$ not significant (ns). Unless otherwise noted, all data points represent independent LNs.

8.8 FUNDING

This work was supported by the NIH grants R01AI134713 (M.Y.G), F31AI161316 (J.Y.H.),

T32GM007270 (J.Y.H.), and T32AI106677 (M.T.C.).

Chapter 9. REFERENCE

Abadie, K., E.C. Clark, R.M. Valanparambil, O. Ukogu, W. Yang, R.M. Daza, K.K.H. Ng, J. Fathima, A.L. Wang, J. Lee, T.H. Nasti, A. Bhandoola, A. Nourmohammad, R. Ahmed, J. Shendure, J. Cao, and H.Y. Kueh. 2024. Reversible, tunable epigenetic silencing of TCF1 generates flexibility in the T cell memory decision. *Immunity* 57:271-286.e213.

Angelosanto, J.M., S.D. Blackburn, A. Crawford, and E.J. Wherry. 2012. Progressive loss of memory T cell potential and commitment to exhaustion during chronic viral infection. *J Virol* 86:8161-8170.

Avery, L., J. Filderman, A.L. Szymczak-Workman, and L.P. Kane. 2018. Tim-3 co-stimulation promotes short-lived effector T cells, restricts memory precursors, and is dispensable for T cell exhaustion. *Proc Natl Acad Sci U S A* 115:2455-2460.

Badovinac, V.P., and J.T. Harty. 2007. Manipulating the rate of memory CD8+ T cell generation after acute infection. *J Immunol* 179:53-63.

Baharom, F., R.A. Ramirez-Valdez, K.K.S. Tobin, H. Yamane, C.A. Dutertre, A. Khalilnezhad, G.V. Reynoso, V.L. Coble, G.M. Lynn, M.P. Mulè, A.J. Martins, J.P. Finnigan, X.M. Zhang, J.A. Hamerman, N. Bhardwaj, J.S. Tsang, H.D. Hickman, F. Ginhoux, A.S. Ishizuka, and R.A. Seder.

2021. Intravenous nanoparticle vaccination generates stem-like TCF1. *Nat Immunol* 22:41-52.

Bangs, D.J., A. Tsitsiklis, Z. Steier, S.W. Chan, J. Kaminski, A. Streets, N. Yosef, and E.A. Robey. 2022. CXCR3 regulates stem and proliferative CD8+ T cells during chronic infection by promoting interactions with DCs in splenic bridging channels. *Cell Rep* 38:110266.

Beltra, J.C., S. Manne, M.S. Abdel-Hakeem, M. Kurachi, J.R. Giles, Z. Chen, V. Casella, S.F. Ngiow, O. Khan, Y.J. Huang, P. Yan, K. Nzingha, W. Xu, R.K. Amaravadi, X. Xu, G.C. Karakousis, T.C. Mitchell, L.M. Schuchter, A.C. Huang, and E.J. Wherry. 2020. Developmental Relationships of Four Exhausted CD8. *Immunity* 52:825-841.e828.

Braun, A., T. Worbs, G.L. Moschovakis, S. Halle, K. Hoffmann, J. Bölter, A. Münk, and R. Förster. 2011. Afferent lymph-derived T cells and DCs use different chemokine receptor CCR7-dependent routes for entry into the lymph node and intranodal migration. *Nat Immunol* 12:879-887.

Bresser, K., L. Kok, A.C. Swain, L.A. King, L. Jacobs, T.S. Weber, L. Perié, K.R. Duffy, R.J. de Boer, F.A. Scheeren, and T.N. Schumacher. 2022. Author Correction: Replicative history marks transcriptional and functional disparity in the CD8. *Nat Immunol* 23:1132.

Brown, H., M.R. Komnick, P.H. Brigleb, T.S. Dermody, and D. Esterházy. 2023. Lymph node sharing between pancreas, gut, and liver leads to immune crosstalk and regulation of pancreatic autoimmunity. *Immunity* 56:2070-2085.e2011.

Buchholz, V.R., M. Flossdorf, I. Hensel, L. Kretschmer, B. Weissbrich, P. Gräf, A. Verschoor, M.

Schiemann, T. Höfer, and D.H. Busch. 2013. Disparate individual fates compose robust CD8+ T cell immunity. *Science* 340:630-635.

Cabeza-Cabrerizo, M., A. Cardoso, C.M. Minutti, M. Pereira da Costa, and C. Reis e Sousa. 2021. Dendritic Cells Revisited. *Annu Rev Immunol* 39:131-166.

Catron, D.M., L.K. Rusch, J. Hataye, A.A. Itano, and M.K. Jenkins. 2006. CD4+ T cells that enter the draining lymph nodes after antigen injection participate in the primary response and become central-memory cells. *J Exp Med* 203:1045-1054.

Chang, J.T., E.J. Wherry, and A.W. Goldrath. 2014. Molecular regulation of effector and memory T cell differentiation. *Nat Immunol* 15:1104-1115.

Chow, M.T., A.J. Ozga, R.L. Servis, D.T. Frederick, J.A. Lo, D.E. Fisher, G.J. Freeman, G.M. Boland, and A.D. Luster. 2019. Intratumoral Activity of the CXCR3 Chemokine System Is Required for the Efficacy of Anti-PD-1 Therapy. *Immunity* 50:1498-1512.e1495.

Combes, A.J., B. Samad, J. Tsui, N.W. Chew, P. Yan, G.C. Reeder, D. Kushnoor, A. Shen, B. Davidson, A.J. Barczak, M. Adkisson, A. Edwards, M. Naser, K.C. Barry, T. Courau, T. Hammoudi, R.J. Argüello, A.A. Rao, A.B. Olshen, ..., and I. Consortium. 2022. Discovering dominant tumor immune archetypes in a pan-cancer census. *Cell* 185:184-203.e119.

Connolly, K.A., M. Kuchroo, A. Venkat, A. Khatun, J. Wang, I. William, N.I. Hornick, B.L.

Fitzgerald, M. Damo, M.Y. Kasmani, C. Cui, E. Fagerberg, I. Monroy, A. Hutchins, J.F. Cheung, G.G. Foster, D.L. Mariuzza, M. Nader, H. Zhao, ..., and N.S. Joshi. 2021. A reservoir of stem-like CD8. *Sci Immunol* 6:eabg7836.

Cruz de Casas, P., K. Knöpper, R. Dey Sarkar, and W. Kastenmüller. 2024. Same yet different - how lymph node heterogeneity affects immune responses. *Nat Rev Immunol* 24:358-374.

De Koker, S., L. Van Hoecke, A. De Beuckelaer, K. Roose, K. Deswarte, M.A. Willart, P. Bogaert, T. Naessens, B.G. De Geest, X. Saelens, B.N. Lambrecht, and J. Grooten. 2017. Inflammatory monocytes regulate Th1 oriented immunity to CpG adjuvanted protein vaccines through production of IL-12. *Sci Rep* 7:5986.

Di Pilato, M., R. Kfuri-Rubens, J.N. Pruessmann, A.J. Ozga, M. Messemaker, B.L. Cadilha, R. Sivakumar, C. Cianciaruso, R.D. Warner, F. Marangoni, E. Carrizosa, S. Lesch, J. Billingsley, D. Perez-Ramos, F. Zavala, E. Rheinbay, A.D. Luster, M.Y. Gerner, S. Kobold, ..., and T.R. Mempel. 2021. CXCR6 positions cytotoxic T cells to receive critical survival signals in the tumor microenvironment. *Cell* 184:4512-4530.e4522.

Duckworth, B.C., F. Lafouresse, V.C. Wimmer, B.J. Broomfield, L. Dalit, Y.O. Alexandre, A.A. Sheikh, R.Z. Qin, C. Alvarado, L.A. Mielke, M. Pellegrini, S.N. Mueller, T. Boudier, K.L. Rogers, and J.R. Groom. 2021. Effector and stem-like memory cell fates are imprinted in distinct lymph node niches directed by CXCR3 ligands. *Nat Immunol* 22:434-448.

Dähling, S., A.M. Mansilla, K. Knöpper, A. Grafen, D.T. Utzschneider, M. Ugur, P.G. Whitney, A. Bachem, P. Arampatzi, F. Imdahl, T. Kaisho, D. Zehn, F. Klauschen, N. Garbi, A. Kallies, A.E. Saliba, G. Gasteiger, S. Bedoui, and W. Kastenmüller. 2022. Type 1 conventional dendritic cells maintain and guide the differentiation of precursors of exhausted T cells in distinct cellular niches. *Immunity* 55:656-670.e658.

Esterházy, D., M.C.C. Canesso, L. Mesin, P.A. Muller, T.B.R. de Castro, A. Lockhart, M. ElJalby, A.M.C. Faria, and D. Mucida. 2019. Compartmentalized gut lymph node drainage dictates adaptive immune responses. *Nature* 569:126-130.

Galon, J., A. Costes, F. Sanchez-Cabo, A. Kirilovsky, B. Mlecnik, C. Lagorce-Pagès, M. Tosolini, M. Camus, A. Berger, P. Wind, F. Zinzindohoué, P. Bruneval, P.H. Cugnenc, Z. Trajanoski, W.H. Fridman, and F. Pagès. 2006. Type, density, and location of immune cells within human colorectal tumors predict clinical outcome. *Science* 313:1960-1964.

Garris, C.S., S.P. Arlauckas, R.H. Kohler, M.P. Trefny, S. Garren, C. Piot, C. Engblom, C. Pfirschke, M. Siwicki, J. Gungabeesoon, G.J. Freeman, S.E. Warren, S. Ong, E. Browning, C.G. Twitty, R.H. Pierce, M.H. Le, A.P. Algazi, A.I. Daud, ..., and M.J. Pittet. 2022. Successful Anti-PD-1 Cancer Immunotherapy Requires T Cell-Dendritic Cell Crosstalk Involving the Cytokines IFN-γ and IL-12. *Immunity* 55:1749.

Gerlach, C., J.C. Rohr, L. Perié, N. van Rooij, J.W. van Heijst, A. Velds, J. Urbanus, S.H. Naik, H. Jacobs, J.B. Beltman, R.J. de Boer, and T.N. Schumacher. 2013. Heterogeneous differentiation

patterns of individual CD8+ T cells. *Science* 340:635-639.

Gerner, M.Y., K.A. Casey, W. Kastenmuller, and R.N. Germain. 2017. Dendritic cell and antigen dispersal landscapes regulate T cell immunity. *J Exp Med* 214:3105-3122.

Gerner, M.Y., W. Kastenmuller, I. Ifrim, J. Kabat, and R.N. Germain. 2012. Histo-cytometry: a method for highly multiplex quantitative tissue imaging analysis applied to dendritic cell subset microanatomy in lymph nodes. *Immunity* 37:364-376.

Gerner, M.Y., P. Torabi-Parizi, and R.N. Germain. 2015. Strategically localized dendritic cells promote rapid T cell responses to lymph-borne particulate antigens. *Immunity* 42:172-185.

Goldberg, M.F., E.K. Roeske, L.N. Ward, T. Pengo, T. Dileepan, D.I. Kotov, and M.K. Jenkins. 2018. Salmonella Persist in Activated Macrophages in T Cell-Sparse Granulomas but Are Contained by Surrounding CXCR3 Ligand-Positioned Th1 Cells. *Immunity* 49:1090-1102.e1097.

Graef, P., V.R. Buchholz, C. Stemberger, M. Flossdorf, L. Henkel, M. Schiemann, I. Drexler, T. Höfer, S.R. Riddell, and D.H. Busch. 2014. Serial transfer of single-cell-derived immunocompetence reveals stemness of CD8(+) central memory T cells. *Immunity* 41:116-126.

Grant, S.M., M. Lou, L. Yao, R.N. Germain, and A.J. Radtke. 2020. The lymph node at a glance - how spatial organization optimizes the immune response. *J Cell Sci* 133:

Grassmann, S., L. Mihatsch, J. Mir, A. Kazeroonian, R. Rahimi, S. Flommersfeld, K. Schober, I. Hensel, J. Leube, L.O. Pachmayr, L. Kretschmer, Q. Zhang, A. Jolly, M.Z. Chaudhry, M. Schiemann, L. Cicin-Sain, T. Höfer, D.H. Busch, M. Flossdorf, and V.R. Buchholz. 2020. Early emergence of T central memory precursors programs clonal dominance during chronic viral infection. *Nat Immunol* 21:1563-1573.

Groom, J.R., J. Richmond, T.T. Murooka, E.W. Sorensen, J.H. Sung, K. Bankert, U.H. von Andrian, J.J. Moon, T.R. Mempel, and A.D. Luster. 2012. CXCR3 chemokine receptor-ligand interactions in the lymph node optimize CD4+ T helper 1 cell differentiation. *Immunity* 37:1091-1103.

Harrell, M.I., B.M. Iritani, and A. Ruddell. 2008. Lymph node mapping in the mouse. *J Immunol Methods* 332:170-174.

Hassett, K.J., I.L. Rajlic, K. Bahl, R. White, K. Cowens, E. Jacquinet, and K.E. Burke. 2024. mRNA vaccine trafficking and resulting protein expression after intramuscular administration. *Mol Ther Nucleic Acids* 35:102083.

Hataye, J., J.J. Moon, A. Khoruts, C. Reilly, and M.K. Jenkins. 2006. Naive and memory CD4+ T cell survival controlled by clonal abundance. *Science* 312:114-116.

Havenar-Daughton, C., D.G. Carnathan, A.V. Boopathy, A.A. Upadhyay, B. Murrell, S.M. Reiss, C.A. Enemuo, E.H. Gebru, Y. Choe, P. Dhadvai, F. Viviano, K. Kaushik, J.N. Bhiman, B. Briney,

D.R. Burton, S.E. Bosinger, W.R. Schief, D.J. Irvine, G. Silvestri, and S. Crotty. 2019. Rapid Germinal Center and Antibody Responses in Non-human Primates after a Single Nanoparticle Vaccine Immunization. *Cell Rep* 29:1756-1766.e1758.

Henning, A.N., R. Roychoudhuri, and N.P. Restifo. 2018. Epigenetic control of CD8. *Nat Rev Immunol* 18:340-356.

Henrickson, S.E., M. Perro, S.M. Loughhead, B. Senman, S. Stutte, M. Quigley, G. Alexe, M. Iannacone, M.P. Flynn, S. Omid, J.L. Jesneck, S. Imam, T.R. Mempel, I.B. Mazo, W.N. Haining, and U.H. von Andrian. 2013. Antigen availability determines $CD8^+$ T cell-dendritic cell interaction kinetics and memory fate decisions. *Immunity* 39:496-507.

Herndler-Brandstetter, D., H. Ishigame, R. Shinnakasu, V. Plajer, C. Stecher, J. Zhao, M. Lietzenmayer, L. Kroehling, A. Takumi, K. Kometani, T. Inoue, Y. Kluger, S.M. Kaech, T. Kurosaki, T. Okada, and R.A. Flavell. 2018. KLRG1. *Immunity* 48:716-729.e718.

Hickman, H.D., G.V. Reynoso, B.F. Ngudiankama, S.S. Cush, J. Gibbs, J.R. Bennink, and J.W. Yewdell. 2015. CXCR3 chemokine receptor enables local CD8(+) T cell migration for the destruction of virus-infected cells. *Immunity* 42:524-537.

Hondowicz, B.D., D. An, J.M. Schenkel, K.S. Kim, H.R. Steach, A.T. Krishnamurty, G.J. Keitany, E.N. Garza, K.A. Fraser, J.J. Moon, W.A. Altemeier, D. Masopust, and M. Pepper. 2016. Interleukin-2-Dependent Allergen-Specific Tissue-Resident Memory Cells Drive Asthma.

Immunity 44:155-166.

Hu, J.K., T. Kagari, J.M. Clingan, and M. Matloubian. 2011. Expression of chemokine receptor CXCR3 on T cells affects the balance between effector and memory CD8 T-cell generation. *Proc Natl Acad Sci U S A* 108:E118-127.

Huang, J.Y., M.R. Lyons-Cohen, and M.Y. Gerner. 2022a. Information flow in the spatiotemporal organization of immune responses. *Immunol Rev* 306:93-107.

Huang, Q., X. Wu, Z. Wang, X. Chen, L. Wang, Y. Lu, D. Xiong, Q. Liu, Y. Tian, H. Lin, J. Guo, S. Wen, W. Dong, X. Yang, Y. Yuan, Z. Yue, S. Lei, Q. Wu, L. Ran, ..., and L. Ye. 2022b. The primordial differentiation of tumor-specific memory CD8. *Cell* 185:4049-4066.e4025.

Im, S.J., M. Hashimoto, M.Y. Gerner, J. Lee, H.T. Kissick, M.C. Burger, Q. Shan, J.S. Hale, T.H. Nasti, A.H. Sharpe, G.J. Freeman, R.N. Germain, H.I. Nakaya, H.H. Xue, and R. Ahmed. 2016. Defining CD8+ T cells that provide the proliferative burst after PD-1 therapy. *Nature* 537:417-421.

Im, S.J., B.T. Konieczny, W.H. Hudson, D. Masopust, and R. Ahmed. 2020. PD-1+ stemlike CD8 T cells are resident in lymphoid tissues during persistent LCMV infection. *Proc Natl Acad Sci U S A* 117:4292-4299.

Irvine, D.J., A. Aung, and M. Silva. 2020. Controlling timing and location in vaccines. *Adv Drug*

Deliv Rev 158:91-115.

Iwata, M., A. Hirakiyama, Y. Eshima, H. Kagechika, C. Kato, and S.Y. Song. 2004. Retinoic acid imprints gut-homing specificity on T cells. *Immunity* 21:527-538.

Jenkins, M.M., H. Bachus, D. Botta, M.D. Schultz, A.F. Rosenberg, B. León, and A. Ballesteros-Tato. 2021. Lung dendritic cells migrate to the spleen to prime long-lived TCF1. *Sci Immunol* 6:eabg6895.

Johnnidis, J.B., Y. Muroyama, S.F. Ngiow, Z. Chen, S. Manne, Z. Cai, S. Song, J.M. Platt, J.M. Schenkel, M. Abdel-Hakeem, J.C. Beltra, A.R. Greenplate, M.A. Ali, K. Nzingha, J.R. Giles, C. Harly, J. Attanasio, K.E. Pauken, B. Bengsch, ..., and E.J. Wherry. 2021. Inhibitory signaling sustains a distinct early memory CD8. *Sci Immunol* 6:

Joshi, N.S., W. Cui, A. Chandele, H.K. Lee, D.R. Urso, J. Hagman, L. Gapin, and S.M. Kaech. 2007. Inflammation directs memory precursor and short-lived effector CD8(+) T cell fates via the graded expression of T-bet transcription factor. *Immunity* 27:281-295.

Kaech, S.M., and W. Cui. 2012. Transcriptional control of effector and memory CD8+ T cell differentiation. *Nat Rev Immunol* 12:749-761.

Kaech, S.M., J.T. Tan, E.J. Wherry, B.T. Konieczny, C.D. Surh, and R. Ahmed. 2003. Selective expression of the interleukin 7 receptor identifies effector CD8 T cells that give rise to long-lived

memory cells. *Nat Immunol* 4:1191-1198.

Kakaradov, B., J. Arsenio, C.E. Widjaja, Z. He, S. Aigner, P.J. Metz, B. Yu, E.J. Wehrens, J. Lopez, S.H. Kim, E.I. Zuniga, A.W. Goldrath, J.T. Chang, and G.W. Yeo. 2017. Early transcriptional and epigenetic regulation of CD8. *Nat Immunol* 18:422-432.

Kalia, V., S. Sarkar, S. Subramaniam, W.N. Haining, K.A. Smith, and R. Ahmed. 2010. Prolonged interleukin-2Ralpha expression on virus-specific CD8+ T cells favors terminal-effector differentiation in vivo. *Immunity* 32:91-103.

Karbach, J., A. Neumann, A. Atmaca, C. Wahle, K. Brand, L. von Boehmer, A. Knuth, A. Bender, G. Ritter, L.J. Old, and E. Jäger. 2011. Efficient in vivo priming by vaccination with recombinant NY-ESO-1 protein and CpG in antigen naive prostate cancer patients. *Clin Cancer Res* 17:861-870.

Kretschmer, L., M. Flossdorf, J. Mir, Y.L. Cho, M. Plambeck, I. Treise, A. Toska, S. Heinzel, M. Schiemann, D.H. Busch, and V.R. Buchholz. 2020. Differential expansion of T central memory precursor and effector subsets is regulated by division speed. *Nat Commun* 11:113.

Krishnaswamy, J.K., U. Gowthaman, B. Zhang, J. Mattsson, L. Szeponik, D. Liu, R. Wu, T. White, S. Calabro, L. Xu, M.A. Collet, M. Yurieva, S. Alsén, P. Fogelstrand, A. Walter, W.R. Heath, S.N. Mueller, U. Yrlid, A. Williams, and S.C. Eisenbarth. 2017. Migratory CD11b. *Sci Immunol* 2:

Krueger, P.D., M.F. Goldberg, S.W. Hong, K.C. Osum, R.A. Langlois, D.I. Kotov, T. Dileepan, and M.K. Jenkins. 2021. Two sequential activation modules control the differentiation of protective T helper-1 (Th1) cells. *Immunity* 54:687-701.e684.

Kurachi, M., J. Kurachi, F. Suenaga, T. Tsukui, J. Abe, S. Ueha, M. Tomura, K. Sugihara, S. Takamura, K. Kakimi, and K. Matsushima. 2011. Chemokine receptor CXCR3 facilitates CD8(+) T cell differentiation into short-lived effector cells leading to memory degeneration. *J Exp Med* 208:1605-1620.

Leal, J.M., J.Y. Huang, K. Kohli, C. Stoltzfus, M.R. Lyons-Cohen, B.E. Olin, M. Gale, and M.Y. Gerner. 2021. Innate cell microenvironments in lymph nodes shape the generation of T cell responses during type I inflammation. *Sci Immunol* 6:

Lee, J.H., H.J. Sutton, C.A. Cottrell, I. Phung, G. Ozorowski, L.M. Sewall, R. Nedellec, C. Nakao, M. Silva, S.T. Richey, J.L. Torres, W.H. Lee, E. Georgeson, M. Kubitz, S. Hodges, T.M. Mullen, Y. Adachi, K.M. Cirelli, A. Kaur, ..., and S. Crotty. 2022. Long-primed germinal centres with enduring affinity maturation and clonal migration. *Nature* 609:998-1004.

Li, J., E. Lu, T. Yi, and J.G. Cyster. 2016. EBI2 augments Tfh cell fate by promoting interaction with IL-2-quenching dendritic cells. *Nature* 533:110-114.

Li, Z., Z.K. Tuong, I. Dean, C. Willis, F. Gaspal, R. Fiancette, S. Idris, B. Kennedy, J.R. Ferdinand, A. Peñalver, M. Cabantous, S. Murtuza Baker, J.W. Fry, G. Carlesso, S.A. Hammond, S.J. Dovedi,

M.R. Hepworth, M.R. Clatworthy, and D.R. Withers. 2022. In vivo labeling reveals continuous trafficking of TCF-1+ T cells between tumor and lymphoid tissue. *J Exp Med* 219:

Lian, J., A.J. Ozga, C.L. Sokol, and A.D. Luster. 2020. Targeting Lymph Node Niches Enhances Type 1 Immune Responses to Immunization. *Cell Rep* 31:107679.

Lin, M.J., J. Svensson-Arvelund, G.S. Lubitz, A. Marabelle, I. Melero, B.D. Brown, and J.D. Brody. 2022. Cancer vaccines: the next immunotherapy frontier. *Nat Cancer* 3:911-926.

Liu, H., K.D. Moynihan, Y. Zheng, G.L. Szeto, A.V. Li, B. Huang, D.S. Van Egeren, C. Park, and D.J. Irvine. 2014. Structure-based programming of lymph-node targeting in molecular vaccines. *Nature* 507:519-522.

Lynn, G.M., R. Laga, P.A. Darrah, A.S. Ishizuka, A.J. Balaci, A.E. Dulcey, M. Pechar, R. Pola, M.Y. Gerner, A. Yamamoto, C.R. Buechler, K.M. Quinn, M.G. Smelkinson, O. Vanek, R. Cawood, T. Hills, O. Vasalatiy, K. Kastenmüller, J.R. Francica, ..., and R.A. Seder. 2015. In vivo characterization of the physicochemical properties of polymer-linked TLR agonists that enhance vaccine immunogenicity. *Nat Biotechnol* 33:1201-1210.

Lyons-Cohen, M.R., E.A. Shamskhou, and M.Y. Gerner. 2024. Site-specific regulation of Th2 differentiation within lymph node microenvironments. *J Exp Med* 221:

Man, K., M. Miasari, W. Shi, A. Xin, D.C. Henstridge, S. Preston, M. Pellegrini, G.T. Belz, G.K.

Smyth, M.A. Febbraio, S.L. Nutt, and A. Kallies. 2013. The transcription factor IRF4 is essential for TCR affinity-mediated metabolic programming and clonal expansion of T cells. *Nat Immunol* 14:1155-1165.

Mandala, S., R. Hajdu, J. Bergstrom, E. Quackenbush, J. Xie, J. Milligan, R. Thornton, G.J. Shei, D. Card, C. Keohane, M. Rosenbach, J. Hale, C.L. Lynch, K. Rupprecht, W. Parsons, and H. Rosen. 2002. Alteration of lymphocyte trafficking by sphingosine-1-phosphate receptor agonists. *Science* 296:346-349.

Martin, J.T., B.L. Hartwell, S.C. Kumarapperuma, M.B. Melo, D.G. Carnathan, B.J. Cossette, J. Adams, S. Gong, W. Zhang, T. Tokatlian, S. Menis, T. Schiffner, C.G. Franklin, B. Goins, P.T. Fox, G. Silvestri, W.R. Schief, R.M. Ruprecht, and D.J. Irvine. 2021. Combined PET and whole-tissue imaging of lymphatic-targeting vaccines in non-human primates. *Biomaterials* 275:120868.

Marzo, A.L., K.D. Klonowski, A. Le Bon, P. Borrow, D.F. Tough, and L. Lefrançois. 2005. Initial T cell frequency dictates memory CD8+ T cell lineage commitment. *Nat Immunol* 6:793-799.

Masopust, D., and J.M. Schenkel. 2013. The integration of T cell migration, differentiation and function. *Nat Rev Immunol* 13:309-320.

Meiser, P., M.A. Knolle, A. Hirschberger, G.P. de Almeida, F. Bayerl, S. Lacher, A.M. Pedde, S. Flommersfeld, J. Hönninger, L. Stark, F. Stögbauer, M. Anton, M. Wirth, D. Wohlleber, K. Steiger, V.R. Buchholz, B. Wollenberg, C.E. Zielinski, R. Braren, ..., and J.P. Böttcher. 2023. A distinct stimulatory cDC1 subpopulation amplifies CD8. *Cancer Cell* 41:1498-1515.e1410.

Mold, J.E., L. Modolo, J. Hård, M. Zamboni, A.J.M. Larsson, M. Stenudd, C.J. Eriksson, G. Durif, P.L. Ståhl, E. Borgström, S. Picelli, B. Reinius, R. Sandberg, P. Réu, C. Talavera-Lopez, B. Andersson, K. Blom, J.K. Sandberg, F. Picard, ..., and J. Frisén. 2021. Divergent clonal differentiation trajectories establish CD8. *Cell Rep* 35:109174.

Nakano, H., K.L. Lin, M. Yanagita, C. Charbonneau, D.N. Cook, T. Kakiuchi, and M.D. Gunn. 2009. Blood-derived inflammatory dendritic cells in lymph nodes stimulate acute T helper type 1 immune responses. *Nat Immunol* 10:394-402.

Nayar, R., E. Schutten, B. Bautista, K. Daniels, A.L. Prince, M. Enos, M.A. Brehm, S.L. Swain, R.M. Welsh, and L.J. Berg. 2014. Graded levels of IRF4 regulate CD8+ T cell differentiation and expansion, but not attrition, in response to acute virus infection. *J Immunol* 192:5881-5893.

Obar, J.J., K.M. Khanna, and L. Lefrançois. 2008. Endogenous naive CD8+ T cell precursor frequency regulates primary and memory responses to infection. *Immunity* 28:859-869.

Oliver, G., J. Kipnis, G.J. Randolph, and N.L. Harvey. 2020. The Lymphatic Vasculature in the 21. *Cell* 182:270-296.

Ozga, A.J., M.T. Chow, M.E. Lopes, R.L. Servis, M. Di Pilato, P. Dehio, J. Lian, T.R. Mempel, and A.D. Luster. 2022. CXCL10 chemokine regulates heterogeneity of the CD8. *Immunity* 55:82-97.e88.

Ozga, A.J., F. Moalli, J. Abe, J. Swoger, J. Sharpe, D. Zehn, M. Kreutzfeldt, D. Merkler, J. Ripoll, and J.V. Stein. 2016. pMHC affinity controls duration of CD8+ T cell-DC interactions and imprints timing of effector differentiation versus expansion. *J Exp Med* 213:2811-2829.

Pais Ferreira, D., J.G. Silva, T. Wyss, S.A. Fuertes Marraco, L. Scarpellino, M. Charmoy, R. Maas, I. Siddiqui, L. Tang, J.A. Joyce, M. Delorenzi, S.A. Luther, D.E. Speiser, and W. Held. 2020. Central memory CD8. *Immunity* 53:985-1000.e1011.

Plumlee, C.R., J.J. Obar, S.L. Colpitts, E.R. Jellison, W.N. Haining, L. Lefrancois, and K.M. Khanna. 2015. Early Effector CD8 T Cells Display Plasticity in Populating the Short-Lived Effector and Memory-Precursor Pools Following Bacterial or Viral Infection. *Sci Rep* 5:12264.

Plumlee, C.R., B.S. Sheridan, B.B. Cicek, and L. Lefrançois. 2013. Environmental cues dictate the fate of individual CD8+ T cells responding to infection. *Immunity* 39:347-356.

Prizant, H., N. Patil, S. Negatu, N. Bala, A. McGurk, S.A. Leddon, A. Hughson, T.D. McRae, Y.R. Gao, A.M. Livingstone, J.R. Groom, A.D. Luster, and D.J. Fowell. 2021. CXCL10. *Cell Rep* 36:109523.

Prokhnevska, N., M.A. Cardenas, R.M. Valanparambil, E. Sobierajska, B.G. Barwick, C. Jansen, A. Reyes Moon, P. Gregorova, L. delBalzo, R. Greenwald, M.A. Bilen, M. Alemozaffar, S. Joshi, C. Cimmino, C. Larsen, V. Master, M. Sanda, and H. Kissick. 2023. CD8. *Immunity* 56:107-124.e105.

Pulendran, B., P. S Arunachalam, and D.T. O'Hagan. 2021. Emerging concepts in the science of vaccine adjuvants. *Nat Rev Drug Discov* 20:454-475.

Rahim, M.K., T.L.H. Okholm, K.B. Jones, E.E. McCarthy, C.C. Liu, J.L. Yee, S.J. Tamaki, D.M. Marquez, I. Tenvooren, K. Wai, A. Cheung, B.R. Davidson, V. Johri, B. Samad, W.E. O'Gorman, M.F. Krummel, A. van Zante, A.J. Combes, M. Angelo, ..., and M.H. Spitzer. 2023. Dynamic CD8. *Cell* 186:1127-1143.e1118.

Ruterbusch, M., K.B. Pruner, L. Shehata, and M. Pepper. 2020. In Vivo CD4. *Annu Rev Immunol* 38:705-725.

Schenkel, J.M., R.H. Herbst, D. Canner, A. Li, M. Hillman, S.L. Shanahan, G. Gibbons, O.C. Smith, J.Y. Kim, P. Westcott, W.L. Hwang, W.A. Freed-Pastor, G. Eng, M.S. Cuoco, P. Rogers, J.K. Park, M.L. Burger, O. Rozenblatt-Rosen, L. Cong, ..., and T. Jacks. 2021. Conventional type I dendritic cells maintain a reservoir of proliferative tumor-antigen specific TCF-1. *Immunity* 54:2338-2353.e2336.

Shakiba, M., P. Zumbo, G. Espinosa-Carrasco, L. Menocal, F. Dündar, S.E. Carson, E.M. Bruno, F.J. Sanchez-Rivera, S.W. Lowe, S. Camara, R.P. Koche, V.P. Reuter, N.D. Socci, B. Whitlock, F. Tamzalit, M. Huse, M.D. Hellmann, D.K. Wells, N.A. Defranoux, ..., and A. Schietinger. 2022. TCR signal strength defines distinct mechanisms of T cell dysfunction and cancer evasion. *J Exp Med* 219:

Shaulov, A., and K. Murali-Krishna. 2008. CD8 T cell expansion and memory differentiation are facilitated by simultaneous and sustained exposure to antigenic and inflammatory milieu. *J Immunol* 180:1131-1138.

Siddiqui, I., K. Schaeuble, V. Chennupati, S.A. Fuertes Marraco, S. Calderon-Copete, D. Pais Ferreira, S.J. Carmona, L. Scarpellino, D. Gfeller, S. Pradervand, S.A. Luther, D.E. Speiser, and W. Held. 2019. Intratumoral Tcf1. *Immunity* 50:195-211.e110.

Smedley, J., B. Turkbey, M.L. Bernardo, G.Q. Del Prete, J.D. Estes, G.L. Griffiths, H. Kobayashi, P.L. Choyke, J.D. Lifson, and B.F. Keele. 2014. Tracking the luminal exposure and lymphatic drainage pathways of intravaginal and intrarectal inocula used in nonhuman primate models of HIV transmission. *PLoS One* 9:e92830.

Soerens, A.G., M. Künzli, C.F. Quarnstrom, M.C. Scott, L. Swanson, J.J. Locquiao, H.E. Ghoneim, D. Zehn, B. Youngblood, V. Vezys, and D. Masopust. 2023. Functional T cells are capable of supernumerary cell division and longevity. *Nature* 614:762-766.

Steele, M.M., A. Jaiswal, I. Delclaux, I.D. Dryg, D. Murugan, J. Femel, S. Son, H. du Bois, C. Hill, S.A. Leachman, Y.H. Chang, L.M. Coussens, N. Anandasabapathy, and A.W. Lund. 2023. Author Correction: T cell egress via lymphatic vessels is tuned by antigen encounter and limits tumor control. *Nat Immunol* 24:729.

Stoltzfus, C.R., J. Filipek, B.H. Gern, B.E. Olin, J.M. Leal, Y. Wu, M.R. Lyons-Cohen, J.Y. Huang, C.L. Paz-Stoltzfus, C.R. Plumlee, T. Pöschinger, K.B. Urdahl, M. Perro, and M.Y. Gerner. 2020. CytoMAP: A Spatial Analysis Toolbox Reveals Features of Myeloid Cell Organization in Lymphoid Tissues. *Cell Rep* 31:107523.

Stoltzfus, C.R., R. Sivakumar, L. Kunz, B.E. Olin Pope, E. Menietti, D. Speziale, R. Adelfio, M. Bacac, S. Colombetti, M. Perro, and M.Y. Gerner. 2021. Multi-Parameter Quantitative Imaging of Tumor Microenvironments Reveals Perivascular Immune Niches Associated With Anti-Tumor Immunity. *Front Immunol* 12:726492.

Tam, H.H., M.B. Melo, M. Kang, J.M. Pelet, V.M. Ruda, M.H. Foley, J.K. Hu, S. Kumari, J. Crampton, A.D. Baldeon, R.W. Sanders, J.P. Moore, S. Crotty, R. Langer, D.G. Anderson, A.K. Chakraborty, and D.J. Irvine. 2016. Sustained antigen availability during germinal center initiation enhances antibody responses to vaccination. *Proc Natl Acad Sci U S A* 113:E6639-E6648.

Tubo, N.J., A.J. Pagán, J.J. Taylor, R.W. Nelson, J.L. Linehan, J.M. Ertelt, E.S. Huseby, S.S. Way, and M.K. Jenkins. 2013. Single naive CD4+ T cells from a diverse repertoire produce different effector cell types during infection. *Cell* 153:785-796.

Utzschneider, D.T., M. Charmoy, V. Chennupati, L. Pousse, D.P. Ferreira, S. Calderon-Copete, M. Danilo, F. Alfei, M. Hofmann, D. Wieland, S. Pradervand, R. Thimme, D. Zehn, and W. Held. 2016. T Cell Factor 1-Expressing Memory-like CD8(+) T Cells Sustain the Immune Response to Chronic Viral Infections. *Immunity* 45:415-427.

Utzschneider, D.T., S.S. Gabriel, D. Chisanga, R. Gloury, P.M. Gubser, A. Vasanthakumar, W. Shi, and A. Kallies. 2020. Early precursor T cells establish and propagate T cell exhaustion in chronic infection. *Nat Immunol* 21:1256-1266.

Waldman, A.D., J.M. Fritz, and M.J. Lenardo. 2020. A guide to cancer immunotherapy: from T cell basic science to clinical practice. *Nat Rev Immunol* 20:651-668.

Wei, F., S. Zhong, Z. Ma, H. Kong, A. Medvec, R. Ahmed, G.J. Freeman, M. Krogsgaard, and J.L. Riley. 2013. Strength of PD-1 signaling differentially affects T-cell effector functions. *Proc Natl Acad Sci U S A* 110:E2480-2489.

Wherry, E.J., and M. Kurachi. 2015. Molecular and cellular insights into T cell exhaustion. *Nat Rev Immunol* 15:486-499.

Wu, T., Y. Ji, E.A. Moseman, H.C. Xu, M. Manglani, M. Kirby, S.M. Anderson, R. Handon, E. Kenyon, A. Elkahloun, W. Wu, P.A. Lang, L. Gattinoni, D.B. McGavern, and P.L. Schwartzberg. 2016. The TCF1-Bcl6 axis counteracts type I interferon to repress exhaustion and maintain T cell stemness. *Sci Immunol* 1:

Wu, Y., J.Y. Huang, M.T. Conlon, M.K. Shenoy, J.L. Chao, M.Y. Chooi, M.A. Koch, and M.Y. Gerner. 2024. Distal Immunization and Systemic Cytokines Establish a Transient Immune Alert State in the Intestine. *J Immunol* 213:373-383.

Yang, C.W., and E.R. Unanue. 2013. Neutrophils control the magnitude and spread of the immune response in a thromboxane A2-mediated process. *J Exp Med* 210:375-387.

Yao, S., B.F. Buzo, D. Pham, L. Jiang, E.J. Taparowsky, M.H. Kaplan, and J. Sun. 2013. Interferon regulatory factor 4 sustains CD8(+) T cell expansion and effector differentiation. *Immunity* 39:833-845.

Youngblood, B., J.S. Hale, H.T. Kissick, E. Ahn, X. Xu, A. Wieland, K. Araki, E.E. West, H.E. Ghoneim, Y. Fan, P. Dogra, C.W. Davis, B.T. Konieczny, R. Antia, X. Cheng, and R. Ahmed. 2017. Effector CD8 T cells dedifferentiate into long-lived memory cells. *Nature* 552:404-409.

Zehn, D., S.Y. Lee, and M.J. Bevan. 2009. Complete but curtailed T-cell response to very low-affinity antigen. *Nature* 458:211-214.

Zhao, T., Y. Cai, Y. Jiang, X. He, Y. Wei, Y. Yu, and X. Tian. 2023. Vaccine adjuvants: mechanisms and platforms. *Signal Transduct Target Ther* 8:283.

Zhou, H., Y. Ma, F. Liu, B. Li, D. Qiao, P. Ren, and M. Wang. 2023. Current advances in cancer vaccines targeting NY-ESO-1 for solid cancer treatment. *Front Immunol* 14:1255799.

Zhou, X., S. Yu, D.M. Zhao, J.T. Harty, V.P. Badovinac, and H.H. Xue. 2010. Differentiation and persistence of memory CD8(+) T cells depend on T cell factor 1. *Immunity* 33:229-240.